

AEROSPACE CORP EL SEGUNDO CA ELECTRONICS RESEARCH LAB F/G 20/5
STUDIES OF BEAM EXPANSION AND DISTRIBUTED BRAGG REFLECTOR LASER--ETC(U)
MAR 81 E M GARMIRE F04701-80-C-0081

TR-0081(6930-03)-1

SD-TR-81-18

NL

1 of 1
AD 1996

END
DATE
FILMED
5-81
DTIC

AD A 097978

Studies of Beam Expansion and Distributed
Bragg Reflector Lasers for Fiber
Optics and Optical Signal Processing

Prepared by
E. M. GARMIRE
Electronics Research Laboratory
Laboratory Operations
The Aerospace Corporation
El Segundo, Calif. 90245

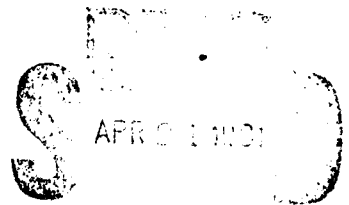
3 March 1981

Interim Report

APPROVED FOR PUBLIC RELEASE;
DISTRIBUTION UNLIMITED

Prepared for
SPACE DIVISION
AIR FORCE SYSTEMS COMMAND
Los Angeles Air Force Station
P.O. Box 92960, Worldway Postal Center
Los Angeles, Calif. 90009

DTIC FILE 037

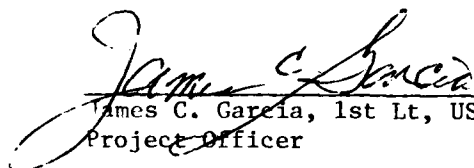


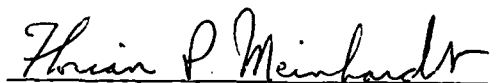
A

This interim report was submitted by The Aerospace Corporation, El Segundo, CA 90245, under Contract No. F04701-80-C-0081 with the Space Division, Deputy for Technology, P.O. Box 92960, Worldway Postal Center, Los Angeles, CA 90009. It was reviewed and approved for The Aerospace Corporation by D.H. Phillips, Director, Electronics Research Laboratory. Lt James C. Garcia, SD/YLVS, was the project officer for the Mission Oriented Investigation and Experimentation Program.

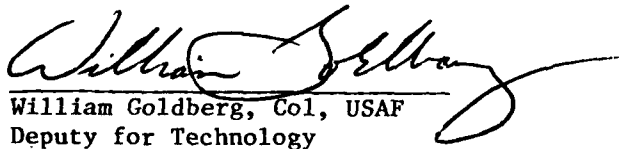
This report has been reviewed by the Public Affairs Office (PAS) and is releasable to the National Technical Information Service (NTIS). At NTIS, it will be available to the general public, including foreign nations.

This technical report has been reviewed and is approved for publication. Publication of this report does not constitute Air Force approval of the report's findings or conclusions. It is published only for the exchange and stimulation of ideas.


James C. Garcia, 1st Lt, USAF
Project Officer


Florian P. Meinhardt, Lt Col, USAF
Director of Advanced Space Development

FOR THE COMMANDER


William Goldberg, Col, USAF
Deputy for Technology

UNCLASSIFIED

SECURITY CLASSIFICATION OF THIS PAGE (When Data Entered)

REPORT DOCUMENTATION PAGE		READ INSTRUCTIONS BEFORE COMPLETING FORM
1. REPORT NUMBER SD-TR-81-18	2. GOVT ACCESSION NO. HD - AC 17 978	3. RECIPIENT'S CATALOG NUMBER
4. TITLE (and Subtitle) STUDIES OF BEAM EXPANSION AND DISTRIBUTED BRAGG REFLECTOR LASERS FOR FIBER OPTICS AND OPTICAL SIGNAL PROCESSING.		5. TYPE OF REPORT & PERIOD COVERED Interim
7. AUTHOR(s) Elsa M. Garmire		6. PERFORMING ORG. REPORT NUMBER TR-0081(6930-03)-1
9. PERFORMING ORGANIZATION NAME AND ADDRESS The Aerospace Corporation El Segundo, Calif. 90245		8. CONTRACT OR GRANT NUMBER(s) F04701-80-C-0081
11. CONTROLLING OFFICE NAME AND ADDRESS Space Division Air Force Systems Command Los Angeles, Calif. 90009		10. PROGRAM ELEMENT, PROJECT, TASK AREA & WORK UNIT NUMBERS
14. MONITORING AGENCY NAME & ADDRESS (if different from Controlling Office)		12. REPORT DATE 3 March 1981
		13. NUMBER OF PAGES 44
		15. SECURITY CLASS. (of this report) Unclassified
		15a. DECLASSIFICATION/DOWNGRADING SCHEDULE
16. DISTRIBUTION STATEMENT (of this Report) Approved for public release; distribution unlimited		
17. DISTRIBUTION STATEMENT (of the abstract entered in Block 20, if different from Report)		
18. SUPPLEMENTARY NOTES		
19. KEY WORDS (Continue on reverse side if necessary and identify by block number) Beam Expansion Distributed Bragg Deflector Distributed Bragg Reflector Lasers Fiber Optics Integrated Optics GaAs Laser Optical Signal Processing Waveguide		
20. ABSTRACT (Continue on reverse side if necessary and identify by block number) Separate studies were performed on beam expansion and on Distributed Bragg Reflector (DBR) lasers preliminary to monolithic integration on GaAs substrates. These components are proposed for use in optical signal processing, for fiber optic sources and for high-brightness lasers.		

DD FORM 1473
(FACSIMILE)

UNCLASSIFIED

SECURITY CLASSIFICATION OF THIS PAGE (When Data Entered)

CONTENTS

INTRODUCTION.....	7
DBR LASER.....	13
WAVEGUIDE BEAM EXPANSION.....	33
REFERENCES.....	47

1

TABLE

I. Data to determine coupling coefficient of grating in DBR lasers..... 13

FIGURES

1. Distributed Bragg deflector.....	8
-------------------------------------	---

FIGURES (Continued)

19. Typical grating fabricated by ion milling through a photolithographically prepared photoresist mask..... 38
20. Semi-logarithmic plot of the near-field Bragg-scattered beam intensity profile of a 90° deflector..... 40
21. Plots of the throughput power, $P_{out}(\theta)$, and Bragg-scattered power, $P_{TMS}(\theta)$ as functions of the input beam polarization angle θ 42
22. Geometry for 45° beam expander along with photographs of an IR television monitor of near field image of guided beam..... 43

INTRODUCTION

The Distributed Bragg Reflector (DBR) laser is a light source compatible with monolithic integrated optics. In the DBR laser one or both cleaved endfaces of a typical double heterostructure laser is replaced by a corrugation at half the wavelength of light in the GaAs. This grating acts as a retro-reflector and replaces the cleave as a laser cavity mirror. The DBR laser can be used as an integrated optics light source for integrated optical circuits.

In this report we described theory and experiments on the DBR laser and on the use of the Distributed Bragg Deflector (DBD) to act as a grating beam expander. The DBD is a corrugation placed at an angle with respect to light emitted from the DBR laser. This grating serves to deflect the incident light through an angle in a distributed fashion, thereby expanding the light beam. This is shown schematically in Fig. 1. The expanded beam travels within the plane of the waveguide and is the basis of several optical circuits, which have application in optical signal processing and optical communications.

The DBR laser and beam expander can be used in rf spectrum analysis. In this application the rf signal modulates a surface acoustic wave, which deflects the guided light in the plane of the waveguide. To achieve high resolution, the guided beam must be several hundred micrometers wide. The beam expander replaces the integrated optical lenses currently being used to produce a guided light beam of sufficient width.

The beam expander can be combined with an output coupler to produce a low beam-divergence laser. This is shown in Fig. 2. The output coupler is a grating corrugation with a spacing which is equal to the wavelength of the propagating light. A grating of this spacing deflects the beam out of the plane of the waveguide and into free space, propagating normal to the plane of the waveguide. Since the deflection is distributed, the beam is expanded by this deflection, and, for apertures about 1 mm in diameter, a diffraction-limited beam 1 mrad in divergence angle will be created. The combination beam expander and output coupler serve as integrated optical telescope and spatial filter. This high brightness laser has applications in point-to-point optical communication systems.

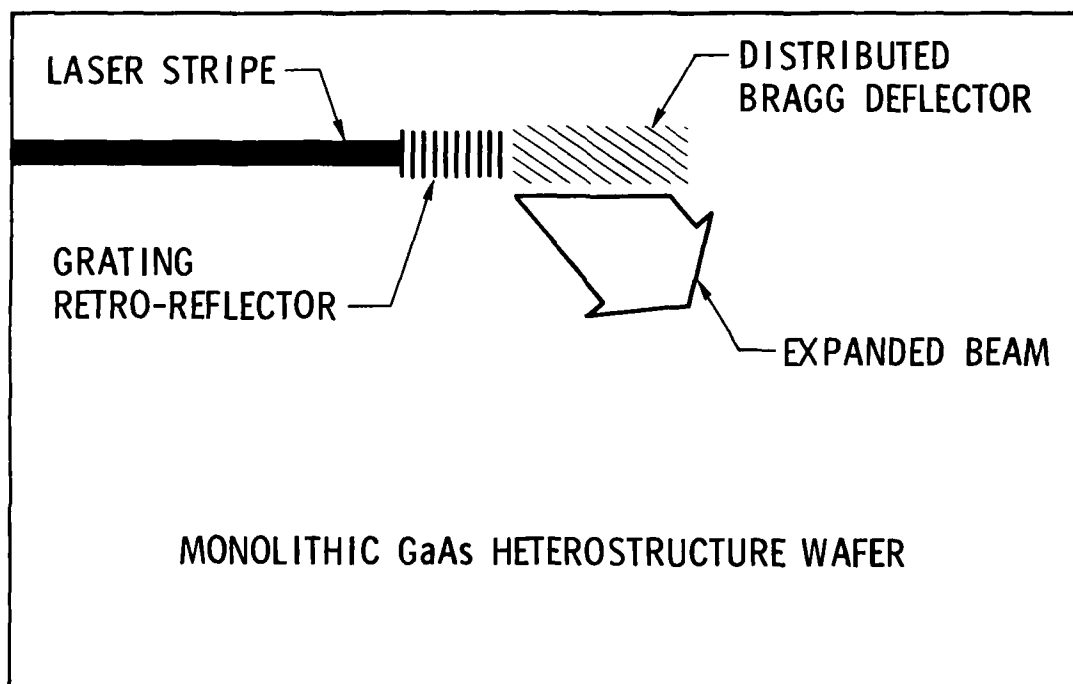


Figure 1 Distributed Bragg Deflector, acting to expand the beam from a DBR laser into a wide beam within the plane of the waveguide for use in optical signal processing.

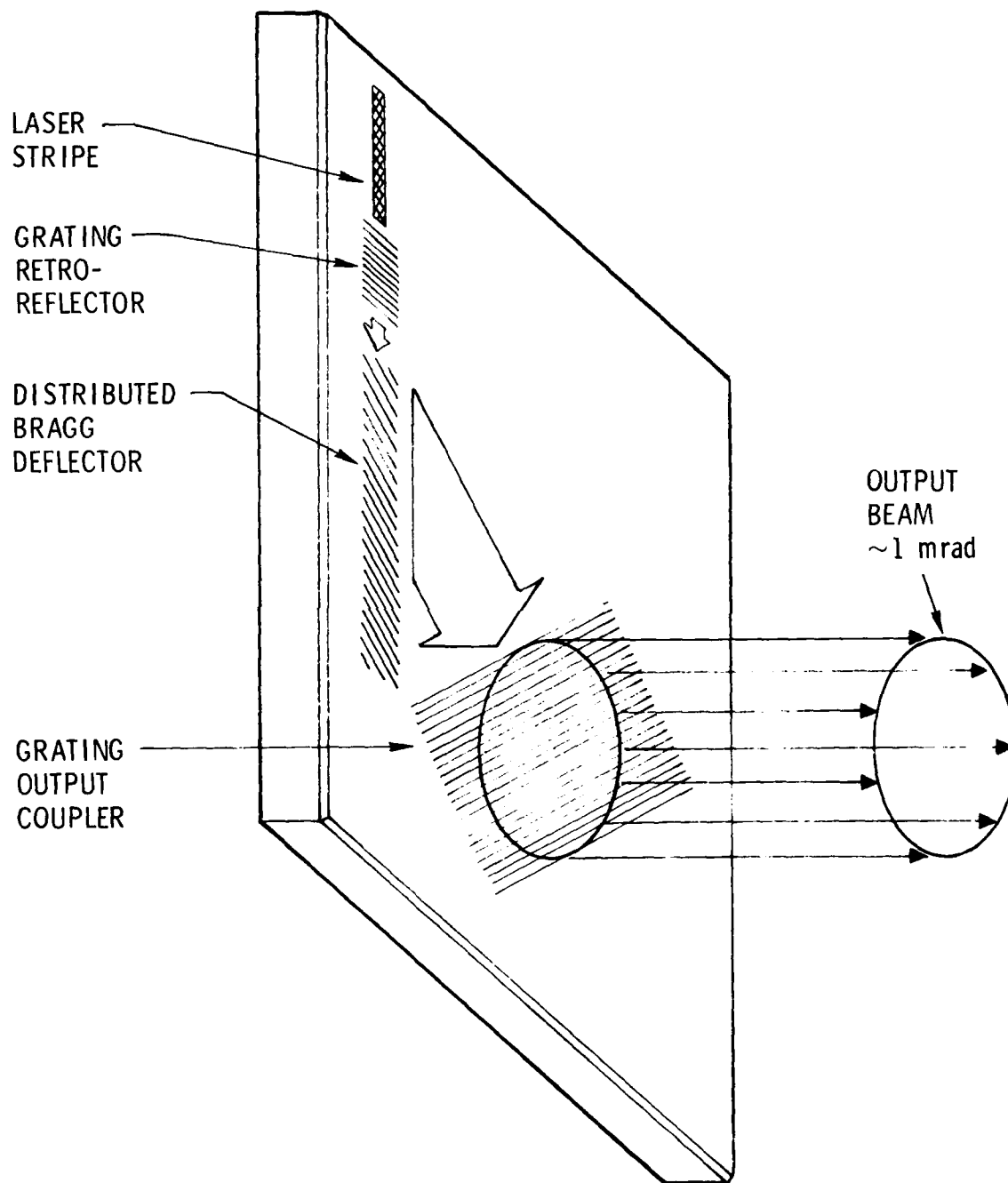


Figure 2 Low beam-divergence laser. The gratings act as an integrated optical spatial filter and telescope.

Applications requiring more power can use the DBD as a power combiner for several laser stripes, as shown in Fig. 3. In design studies, it has been shown that 1 Watt with a 1 mrad radiance angle is possible.

The DBR laser, beam expander and output coupler are useful in fiber optics applications. The expansion factor can be chosen so that a fiber can be butt-coupled to the output coupler, producing a match between the numerical aperture of the fiber and the emission pattern of the grating coupler. This is shown in Fig. 4. The fiber attaches to the face of the wafer, reducing alignment tolerances.

In this report we discuss experiments performed on DBR laser and on the beam expander, with emphasis on its usefulness for fiber optics and signal processing applications.

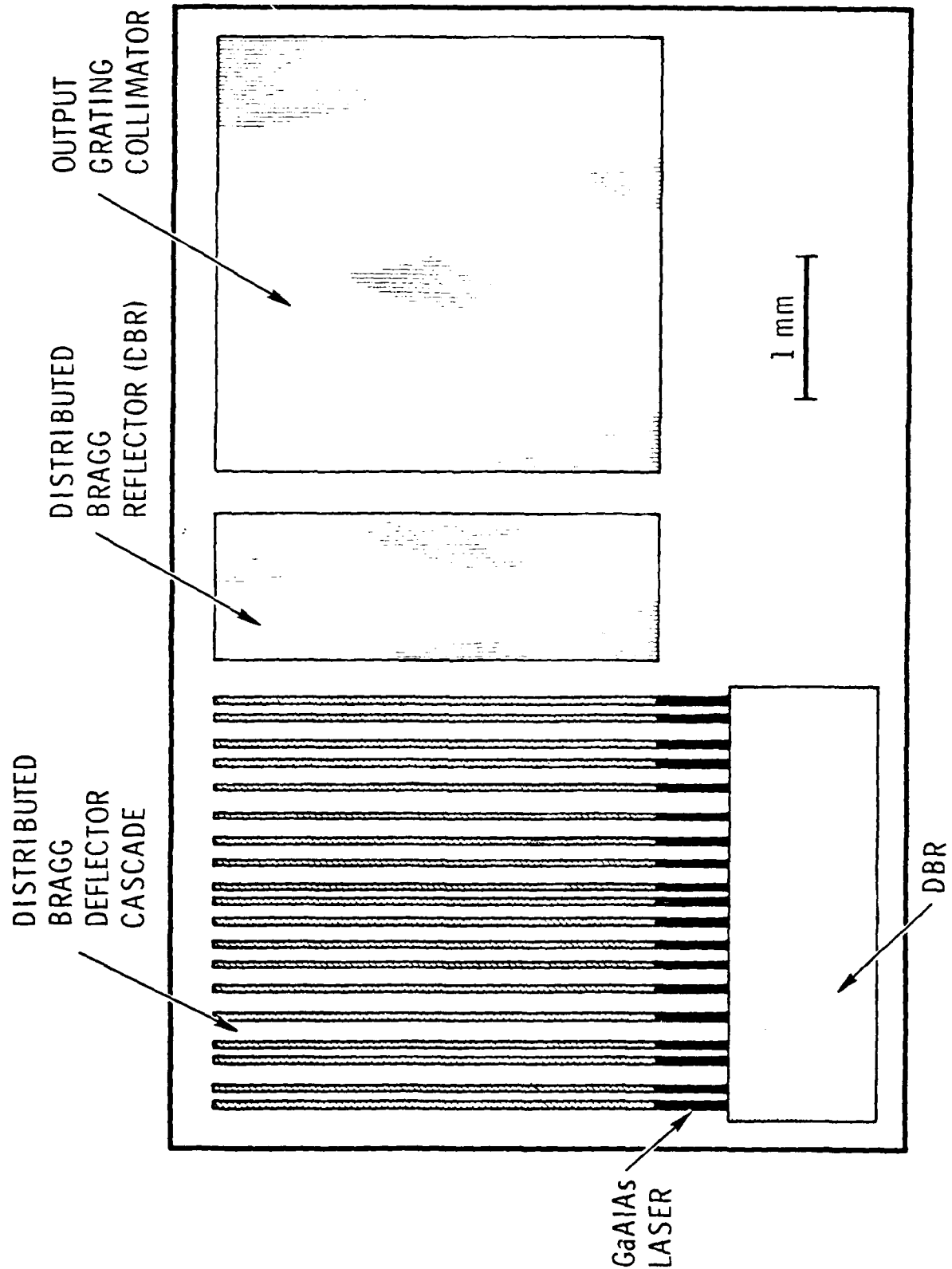


Figure 3 High Brightness Laser

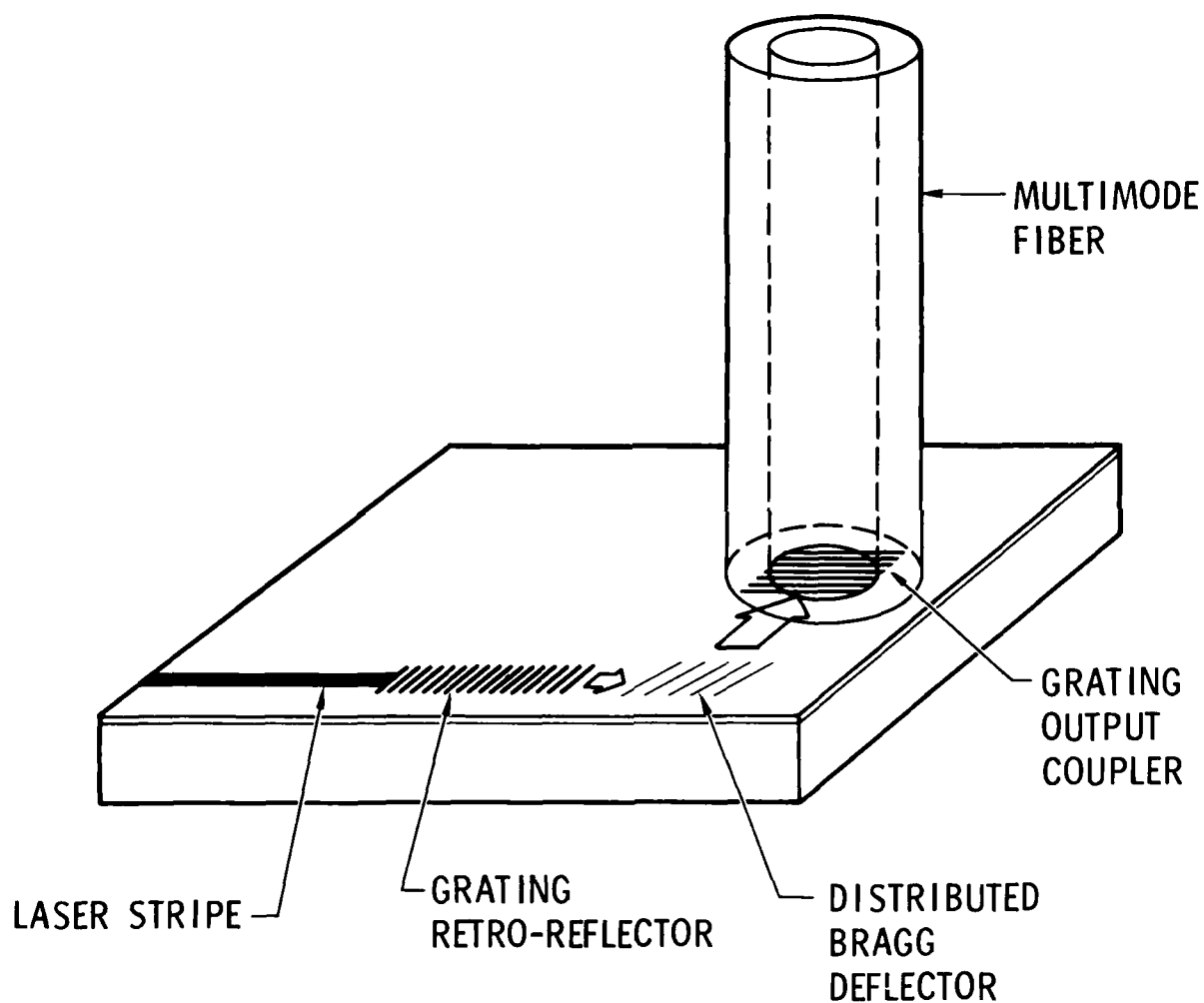


Figure 4 Distributed Bragg Deflector plus grating output coupler used to shape the beam from a stripe geometry laser to the mode pattern of a multi-mode fiber. The fiber attaches to the surface of the GaAs double heterostructure wafer, in a fashion analogous to the Burrus diode.

DBR LASERS

The cross section geometry of the DBR lasers which were fabricated is shown in Fig. 5. The gratings were third order, and the laser region was a large optical cavity. The layer structure shown was not optimum, because the waveguide region was thicker than desired, but was the best material available at the time.

Measurements were made of the front-to-rear power ratio of DBR lasers of differing lengths to determine the coupling coefficient of the grating and to check for its reproducibility. Two devices were compared in detail; the data is shown in Table I.

Table I

Data to determine coupling coefficient of gratings in DBR lasers

Sample Number	g ⁹	g ⁵
Power out grating (mW)	1	0.5
Power out cleave (mW)	30	10
Power ratio (grating to cleave), T	0.03	0.05
Ln T/4	-5.0	-4.4
Grating Length	1000 μm	464 μm
K (μm^{-1})	0.0024	0.0047
$L_g = (2K)^{-1}$	205 μm	106 μm

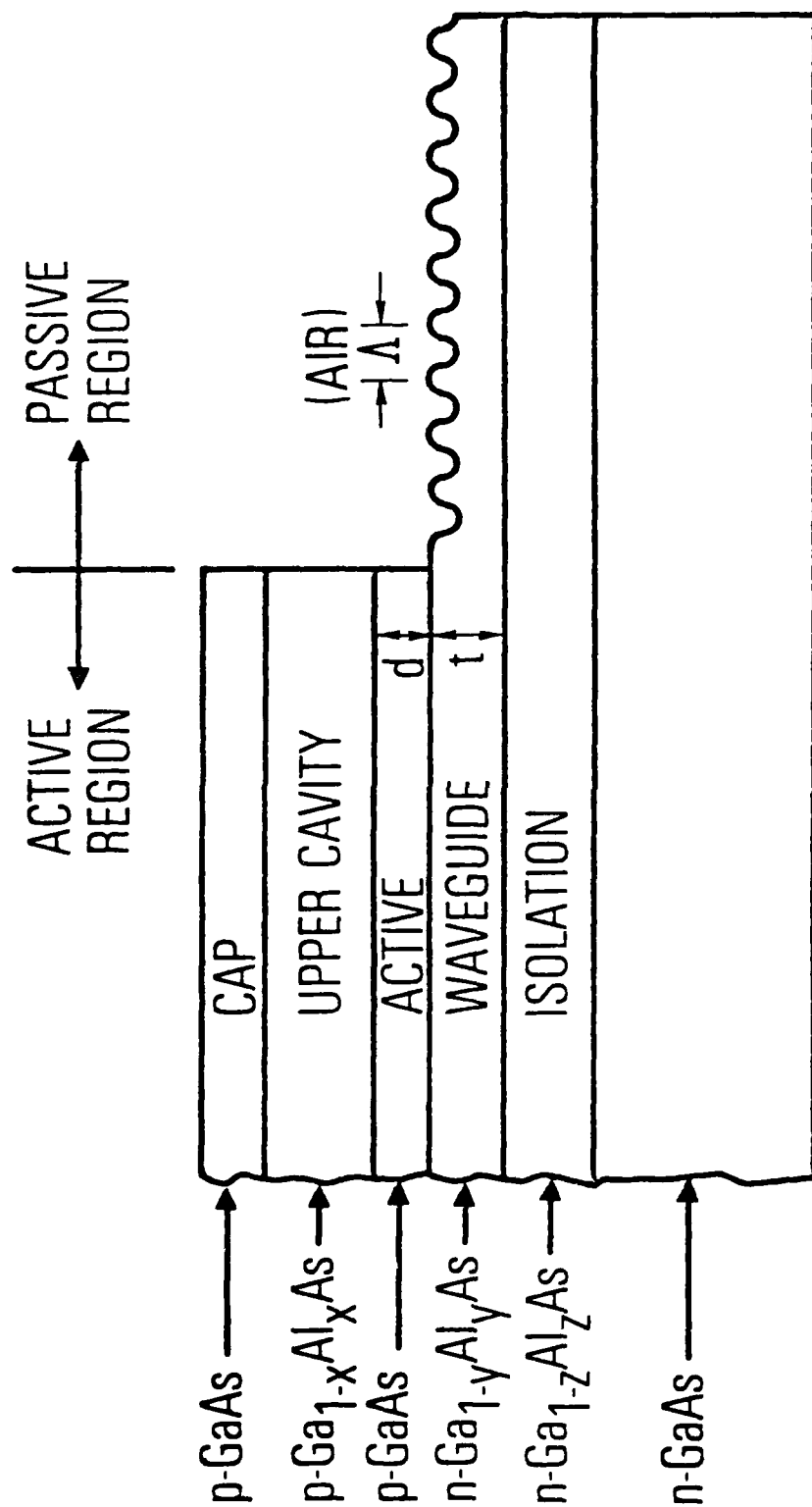


Figure 5 Geometry of the DBR laser fabricated and studied. The important parameters are $d = 0.25 \mu\text{m}$, $t = 1.68 \mu\text{m}$, $x = 0.26$, $y = 0.1$, $z = 0.34$, $\Lambda = 0.36$.

According to the theory, a grating retro-reflector of length L on resonance has the following behavior for transmission and reflection:

Transmission:

$$T = \frac{1}{\cosh^2 KL} \quad (1)$$

Reflection:

$$R = \frac{\sinh^2 KL}{\cosh^2 KL} \quad (2)$$

When $KL \gg 1$:

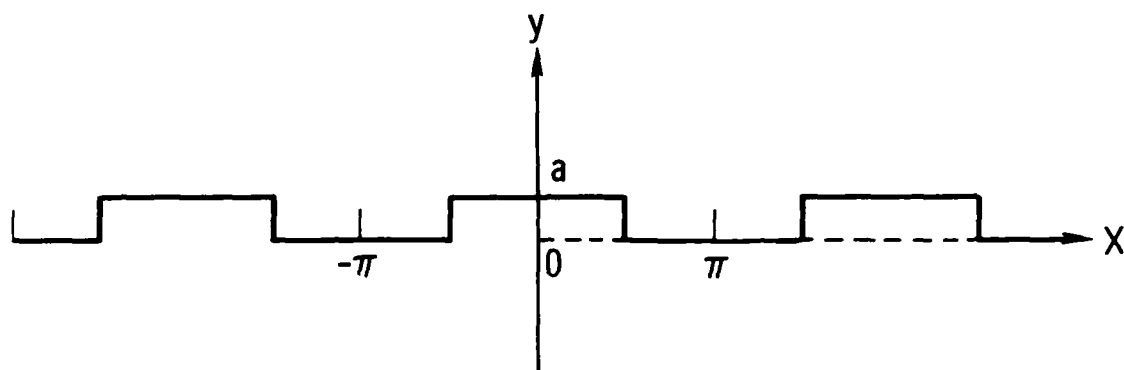
$$T = 4e^{-2KL}, \quad R = 1 - T. \quad (3)$$

The coupling coefficient was determined from Eq. (3) using the fact that the front-to-back power ratio will be the same as the transmission of the grating. The results are shown in Table 1. Although the values of K differ by a factor of two, we feel this is well within experimental error. The average coupling coefficient is $K = 0.0035 \mu\text{m}^{-1}$. We now compare these measurements with theoretical expectations.

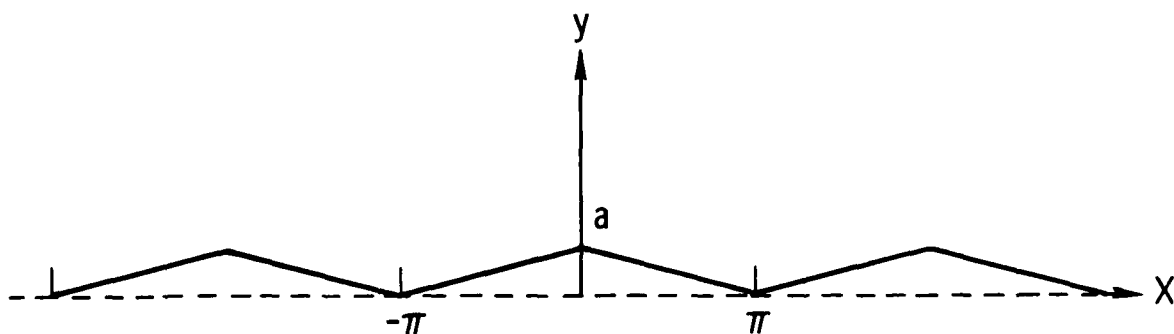
Coupled mode theory predicts that a corrugated waveguide couple forward and backward waveguide modes with a coupling coefficient K . Light originally travelling forward transfers to the backward wave exponentially with length, with a coefficient given by K . Thus the effectiveness of a grating can be described by describing its coupling coefficient. For square corrugations of depth d the coupling coefficient is ⁽¹⁾

$$K = \frac{2\pi^2 (n^2 - 1)}{3 m \lambda n} \left(\frac{d}{t}\right)^3 \quad (4)$$

where n is the refractive index of the guide, t is the thickness of the waveguide and m is the mode number. A related parameter is the characteristic distance at which the power in the initial mode decreases by a factor of $1/e$. This characteristic length is given by $L_g = (2K)^{-1}$. The experimental grating looked more like triangular teeth than square teeth, however. The comparison between square and triangular shapes may be made by comparing the fourier transforms for the third order coefficients for square and triangular shapes. Using the calculations shown in Fig. 6, we see that the polarization induced by a triangular grating will be $2/3$ that induced by the step index. Thus we expect the grating coupling coefficient to be



$$F = \int_{-\pi}^{\pi} y(x) \cos 3x \, dx = a \int_{-\pi/2}^{\pi/2} \cos 3x \, dx = \frac{2a}{3}$$



$$F = \int y(x) \cos 3x \, dx = -2a \int_0^{\pi} x \cos 3x \, dx = \frac{4a}{9}$$

Figure 6 Geometry and calculations used to determine effectiveness of triangular teeth compared to square teeth in producing feedback.

$$K = \frac{4\pi^2(n^2-1)}{9m\lambda n} \left[\frac{d}{t_e} \right]^3 \quad (5)$$

where we have taken Eq. 4, multiplied by 2/3 and used t_e , the effective guided mode thickness, instead of t , for guides which are not infinitely well confining.

From SEM photographs of the grating, we estimate $d = \Lambda/3$, $t = 1.68 \mu\text{m}$, $\Lambda =$ the grating periodicity $= 0.36 \mu\text{m}$. The grating was used in third order, and the refractive index of GaAs at $0.88 \mu\text{m}$ is 3.59. These numbers give the theoretically expected coupling coefficient of $K = 0.0059 \mu\text{m}^{-1}$. In order to calculate this number, it was required to know the effective guide width. This was determined by solving the eigenvalue equation for the waveguide to determine the exponential profile outside of the guide, γ , and calculate $t_e = t + 1/\gamma$. For the DBR lasers, the V parameter for the waveguide was $\Delta k_0^2 t^2 = 146$, resulting in two modes, given by the following eigenvalue equation:

$$\tan u = - \left(\frac{146}{u^2} - 1 \right)^{-1/2} \quad \text{where } u = k_t t$$

The solutions are $k_t t = 2.9, 5.8$, and give $\gamma t = 12$ for both modes. This makes the effective thickness $= 1.75 \mu\text{m}$ for both. This is the value used in Eq. (5) to determine the theoretical coupling coefficient. The calculated value of 0.0059 agrees within experimental error with the measured value of .0035. The agreement between theory and experiment allows us to predict behavior for other waveguides. For example, material with waveguide thickness of $0.6 \mu\text{m}$ should yield devices with coupling coefficients as much as eight times larger.

Other properties relevant to DBR lasers as sources for fiber optics, high brightness lasers and optical signal processing by monolithic integrated optics were investigated. These include the spectrum, total power, the P-I characteristics, and the beam divergences in both planes, including whether or not the light was diffraction limited. The results are summarized here. A

typical spectrum of a DBR laser is shown in Fig. 7. First, in order to prove that the laser action occurred from the grating and not from spurious reflections the following tests were applied. First, it was observed that the spectrum was a single mode. Comparable spectra for Fabry-Perot lasers from the same material were multimode, as shown in Fig. 8. Secondly, a DBR laser which operated at room temperature was cooled to liquid nitrogen temperature, and laser action ceased, since the reflectivity of the grating was no longer at the frequency of the fluorescence. This is in contrast to Fabry-Perot lasers whose frequency shifts and threshold lowers with temperature.

In some of the diodes two lines occurred, as shown in Fig. 9. This occurred because the waveguide was sufficiently thick that not only the lowest even mode, but also the lowest odd mode could be confined in the passive region. These modes are shown in Fig. 10, and occur in the following way.

The laser wavelength is determined by the condition that the corrugation spacing is in resonance with the longitudinal propagation vector: i.e. $k_z = 3\pi/\Lambda$. However, the different modes have different propagation constants since the transverse propagation constant is different for each mode. The dispersion relation thus becomes

$$k_z^2 = n_g^2 k_o^2 - \left(\frac{(m+1)\pi}{t_e} \right)^2. \quad (6)$$

To get a simple expression for the difference in frequencies for DBR laser lines operating on different waveguide modes, assume that the effective waveguide thickness is independent of mode, that the refractive index does not depend on frequency, and that the difference in wavelength between the two laser modes is much less than the wavelength. Then the equation for laser wavelength, given by

$$\left(\frac{3}{\Lambda} \right)^2 = \frac{4n_g^2}{\lambda^2} - \left(\frac{m+1}{t_e} \right)^2$$

can be differentiated, yielding,

$$\Delta\lambda = \frac{3\lambda^3}{8t_e^2 n_g^2}. \quad (7)$$

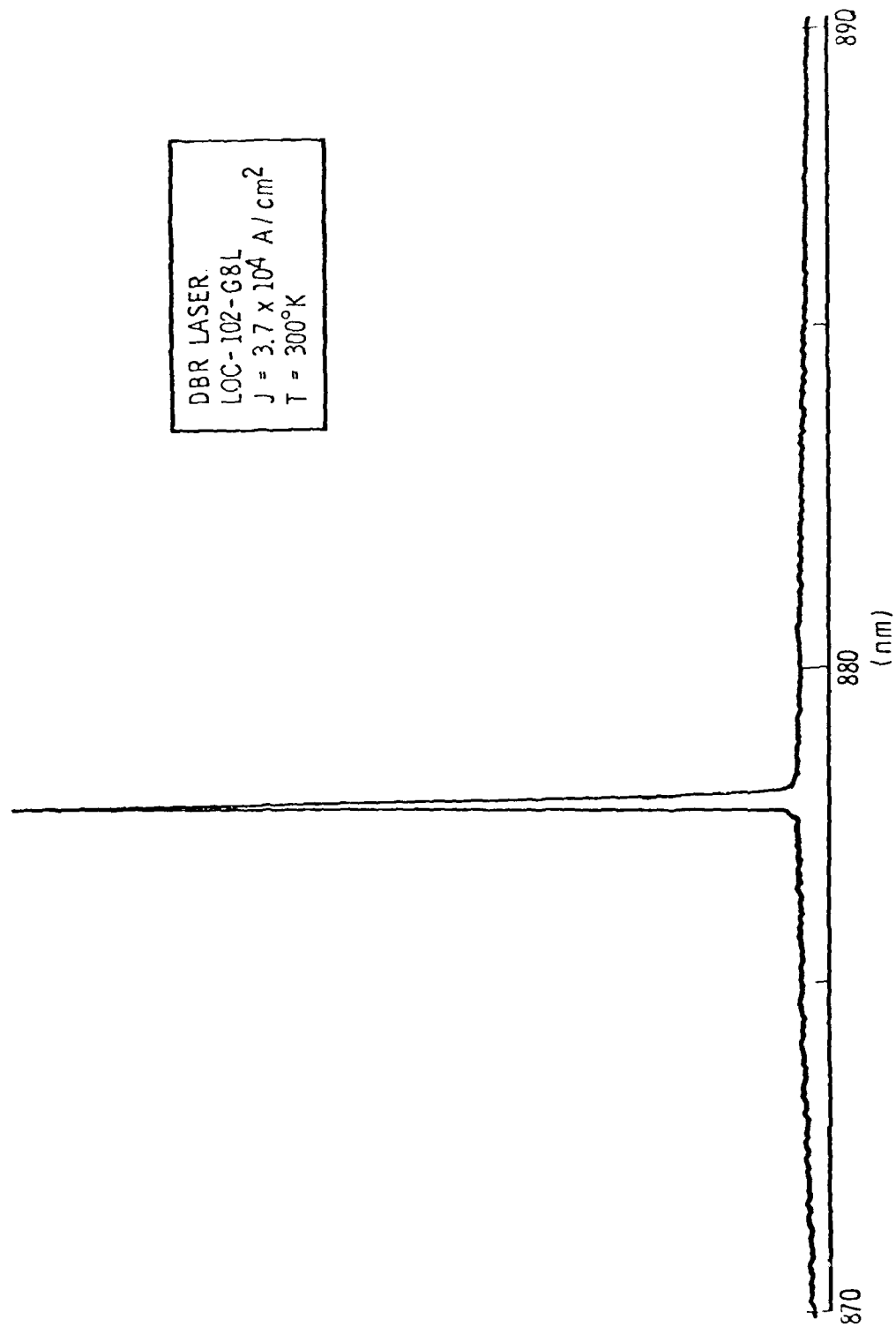
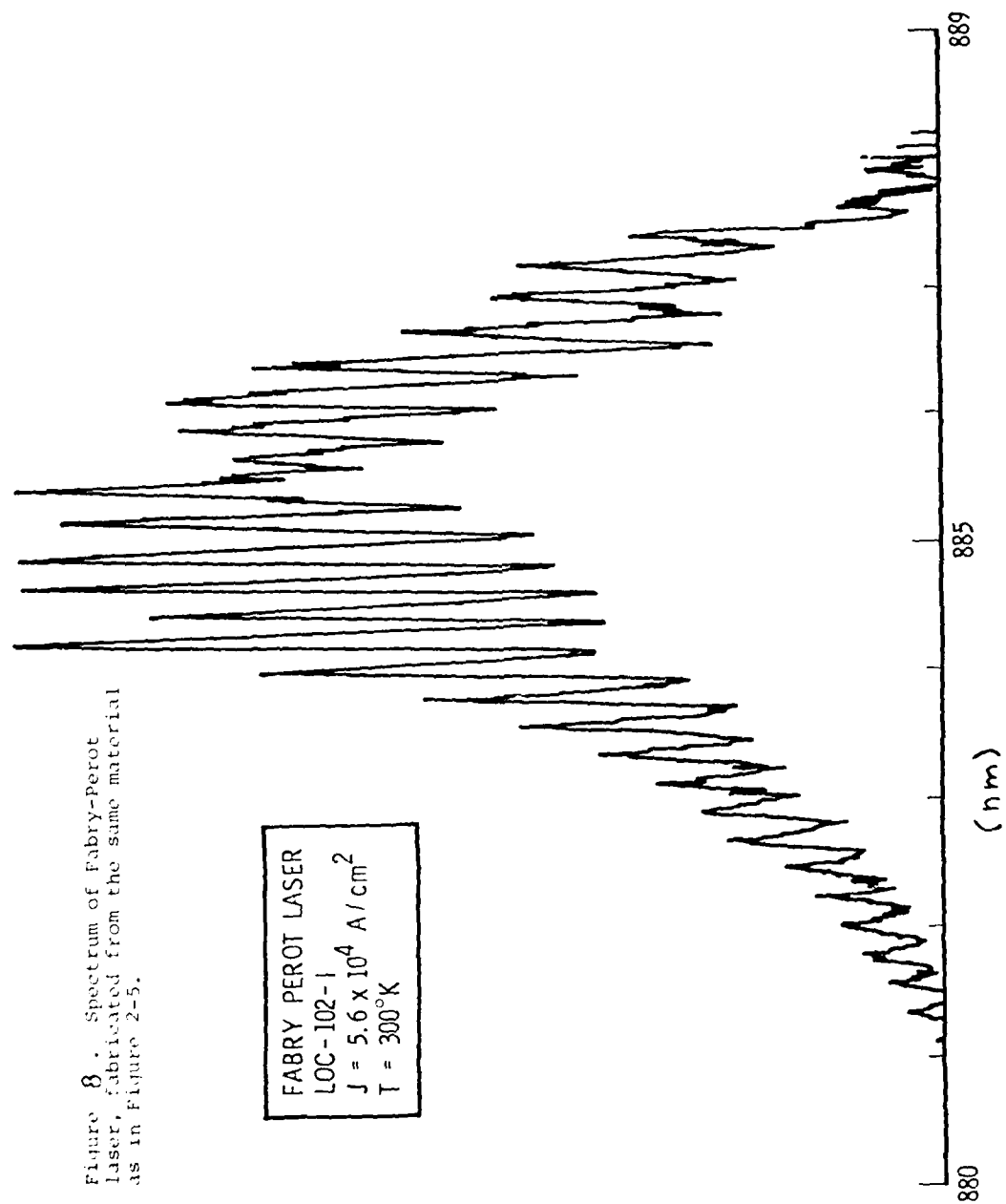


Figure 7 Spectrum of typical DBR laser.

Figure 8 . Spectrum of Fabry-Perot laser, fabricated from the same material as in Figure 2-5.



DBR LASER
LOC-102-G9
 $J = 9.26 \times 10^4 \text{ A/cm}^2$
 $T = 300^\circ\text{K}$

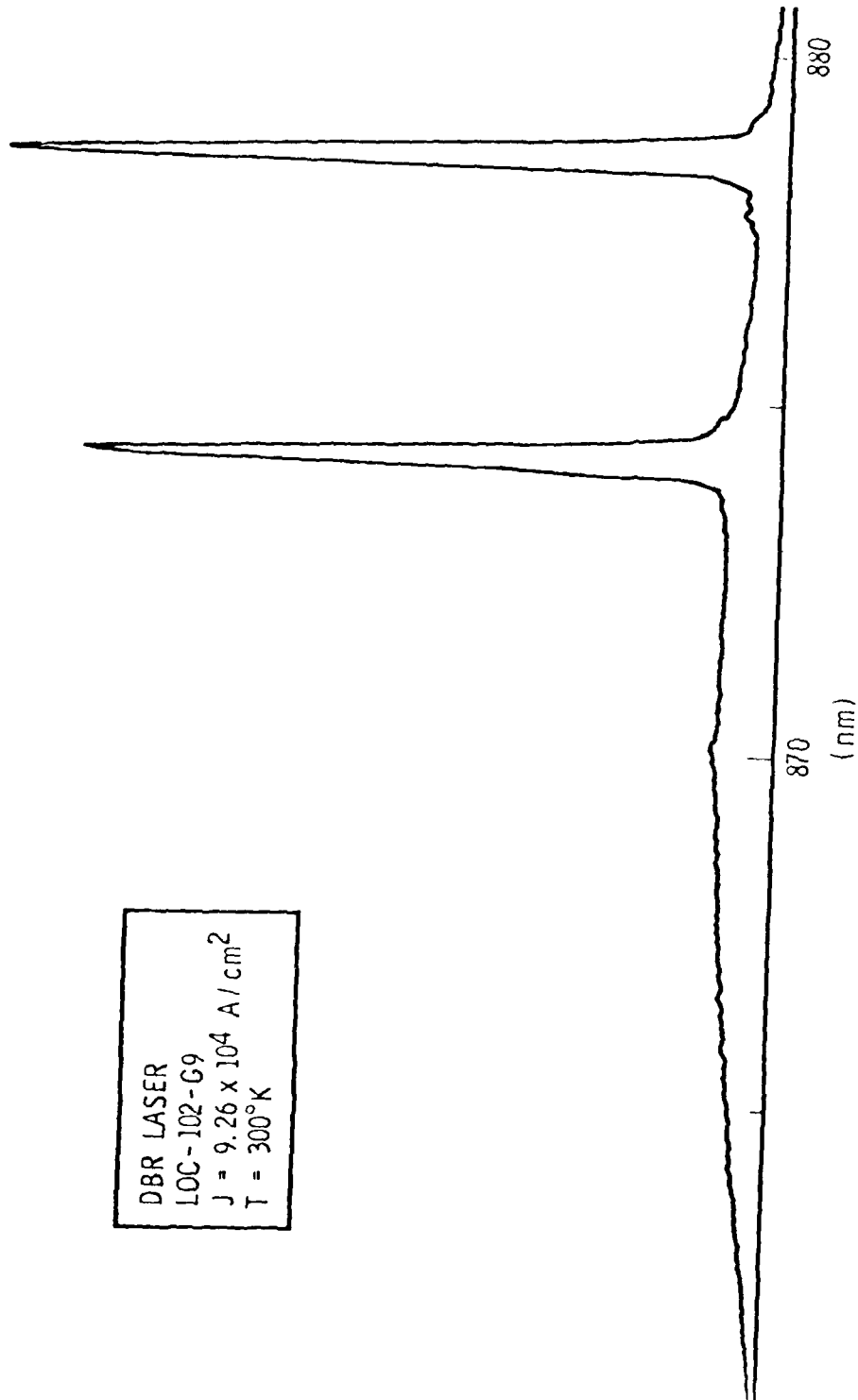


Figure 9 Spectrum of DBR laser which supports two waveguide modes and therefore has two oscillation frequencies.

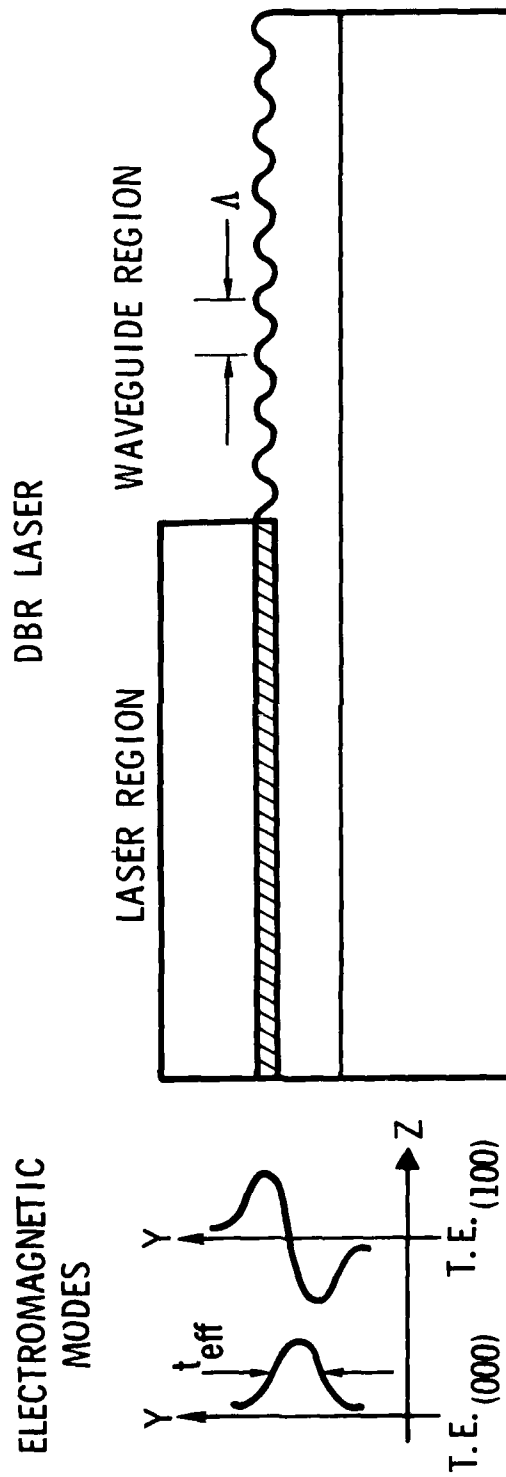


Figure 10 DBR laser geometry, showing the two TE modes which exist in the DBR laser when the waveguide layer is fairly thick. Each of these modes has a different longitudinal propagation constant and therefore oscillates at a different frequency.

The refractive index which comes into the calculation of laser modes is the effective index:

$$n_{\text{eff}} = n + v \, dn/dv \approx 4.8$$

For an effective waveguide thickness of $1.75 \, \mu\text{m}$, the difference in wavelength between modes should be 35\AA . In devices tested, the actual difference between modes was 40\AA . We consider this good agreement, to within the accuracy to which t_e is known. Finally, as further check on this explanation of the two output frequencies, we measured their far field mode profiles separately. We observed that the longer wavelength oscillation was in the lowest order spatial mode, while the shorter wavelength oscillation had a double-humped far field profile, proving that it was indeed oscillating in the higher order waveguide mode.

The linewidths just above laser threshold were typically about 1\AA . Diode G8, shown in Fig. 7, had a width of about $1.1 \, \text{\AA}$, and diode G9, shown in Fig. 11a, had a width of $1.6 \, \text{\AA}$. The apparent linewidth broadened slightly with pumping, as shown in Fig. 11b, in which diode g5 is pumped three times threshold. The line had broadened to about $3 \, \text{\AA}$. It was observed on the oscilloscope that the frequency changed during the $100 \, \text{nsec}$ of the input pulse. The broadening was a chirp effect due to heating in the junction. Such effects have been seen before in Fabry-Perot diodes, but here are much smaller because of the smaller temperature sensitivity of DBR lasers.

Diode g9 had a complicated behavior, since the two frequencies corresponding to two guided modes occurred at high pumping rates. It was observed that at low excitation levels the shorter wavelength was the strongest peak and the longer wavelength occurred only during the initial portion of the pulse. Evidently heating caused the resonance condition to change and near the end of the pulse the shorter wavelength had a lower threshold and was the only frequency above threshold. This data demonstrates that even when a grating is used, it is possible to get several wavelengths oscillating, not necessarily simultaneously in time within the laser. Clearly DBR diodes must be optimized to have well-behaved results.

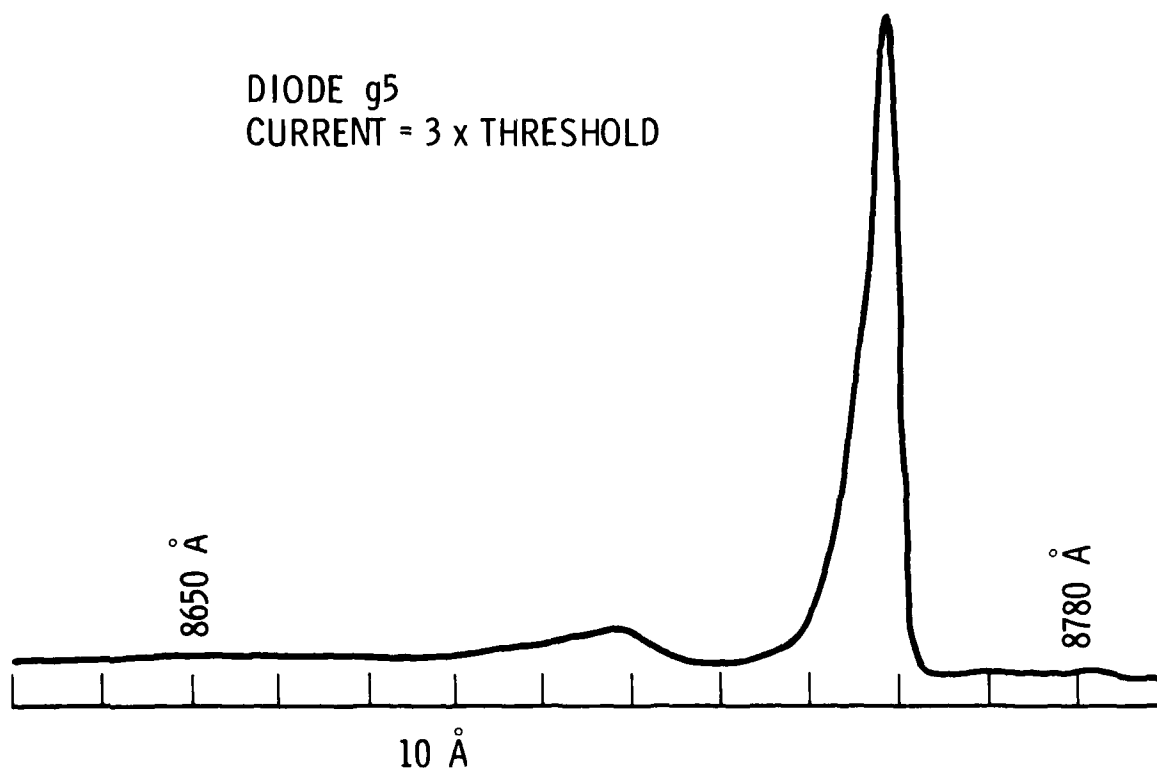
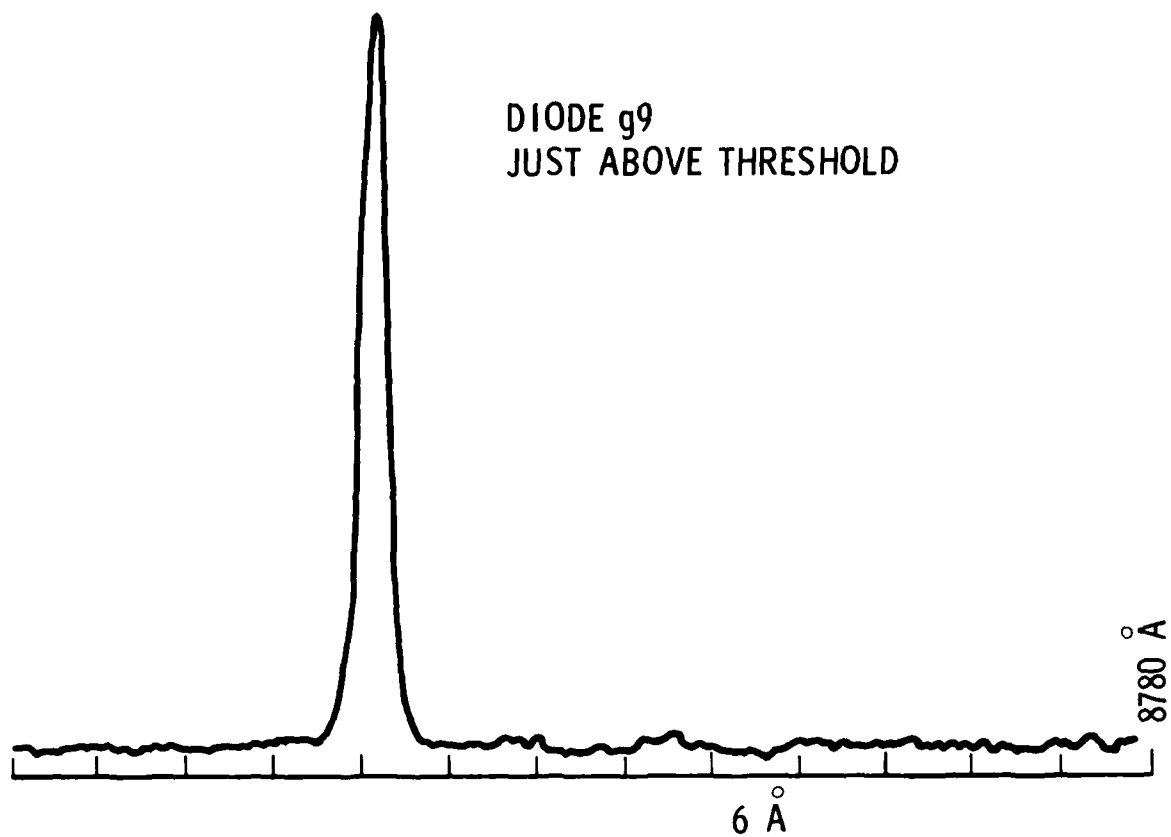


Figure 11 Spectra of two DBR lasers

The complexity of this device can be seen from the P-I curve (Fig. 12), which are filled with kinks. The DBR laser causes only one or two frequencies to oscillate, but does not necessarily improve P-I characteristics over Fabry-Perot lasers.

Since kinks seem to be related to the filamentary structure of lasers, and since we were interested in beam quality in order to perform beam expansion, we made a careful study of the diffraction qualities of the light emitted from the DBR lasers. Depending on the device, we were able to observe diffraction limited operation, just above threshold. This is demonstrated by studying the divergence of sample g9, right above threshold. Near field patterns were observed both out the cleave and the grating face (Fig. 13). In addition, the in-plane beam divergence was measured coming out of the cleave. This was done by monitoring the spot size as a function of distance from the cleave. The data are shown in Fig. 14.

The data are analyzed by comparing the measured divergence with that expected for a Gaussian beam of the width determined from the near field intensity profiles (Fig. 13). The angular divergence of a Gaussian beam is given by

$$\theta_0 = \lambda / \pi \omega_0$$

where θ_0 is the half-angle and ω_0 is the half width of the beam at $1/e^2$ in intensity.

Redefining the quantities in terms of full width half maximum,

$$\theta = \frac{\lambda}{0.72\pi\omega}.$$

The filament measured in the near field had an apparent width of $6.4 \mu\text{m}$ (correction has not been made for resolution of the microscope objective used in this measurement). The far field beam divergence out the cleave was 0.072 rad , which corresponds to the diffraction expected from a filament of width $5.4 \mu\text{m}$. This is in good agreement with the measured filament width, and supports the assumption that this laser operated in a single spatial mode.

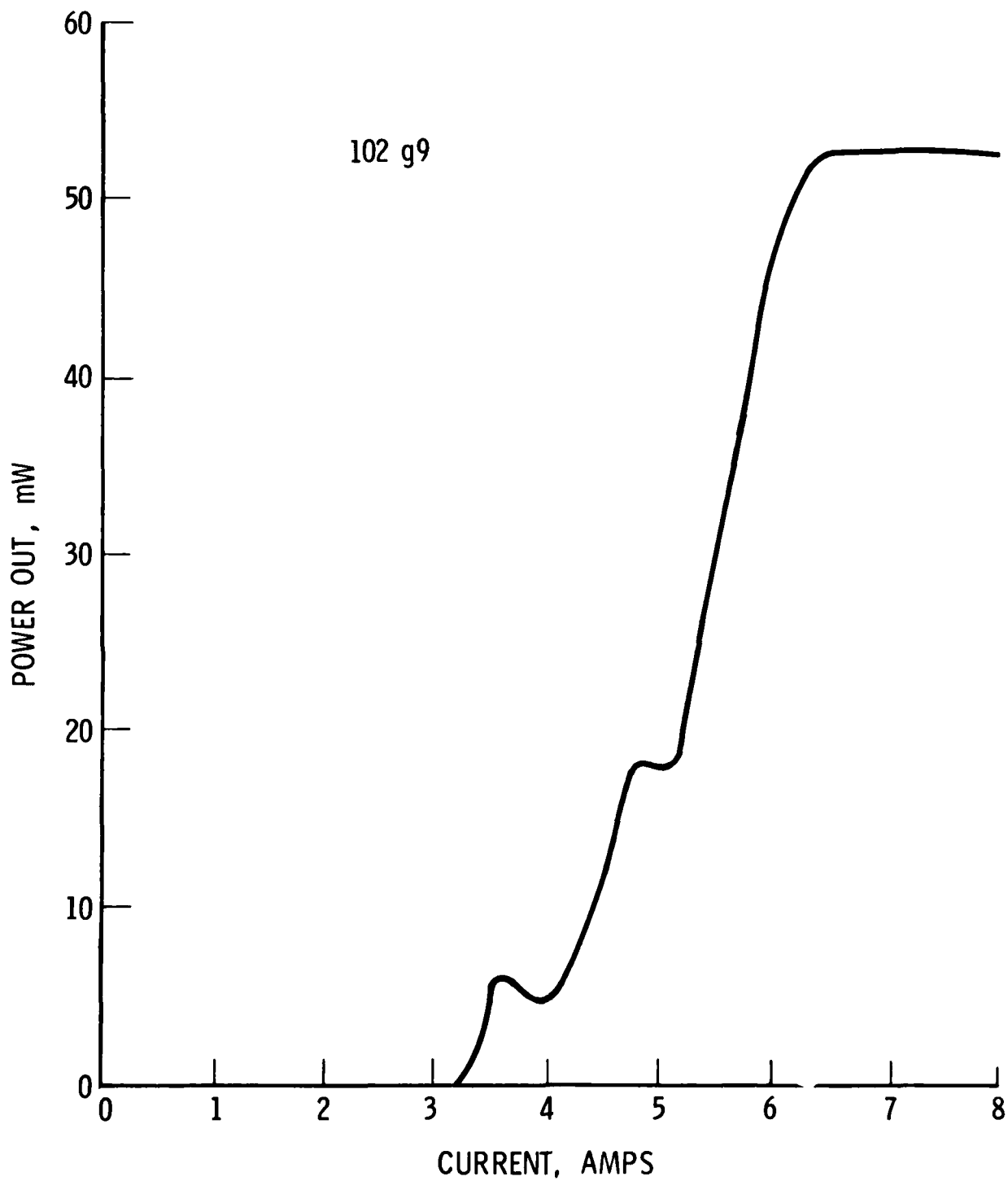


Figure 12 Total light power out as a function of total current to the diode.

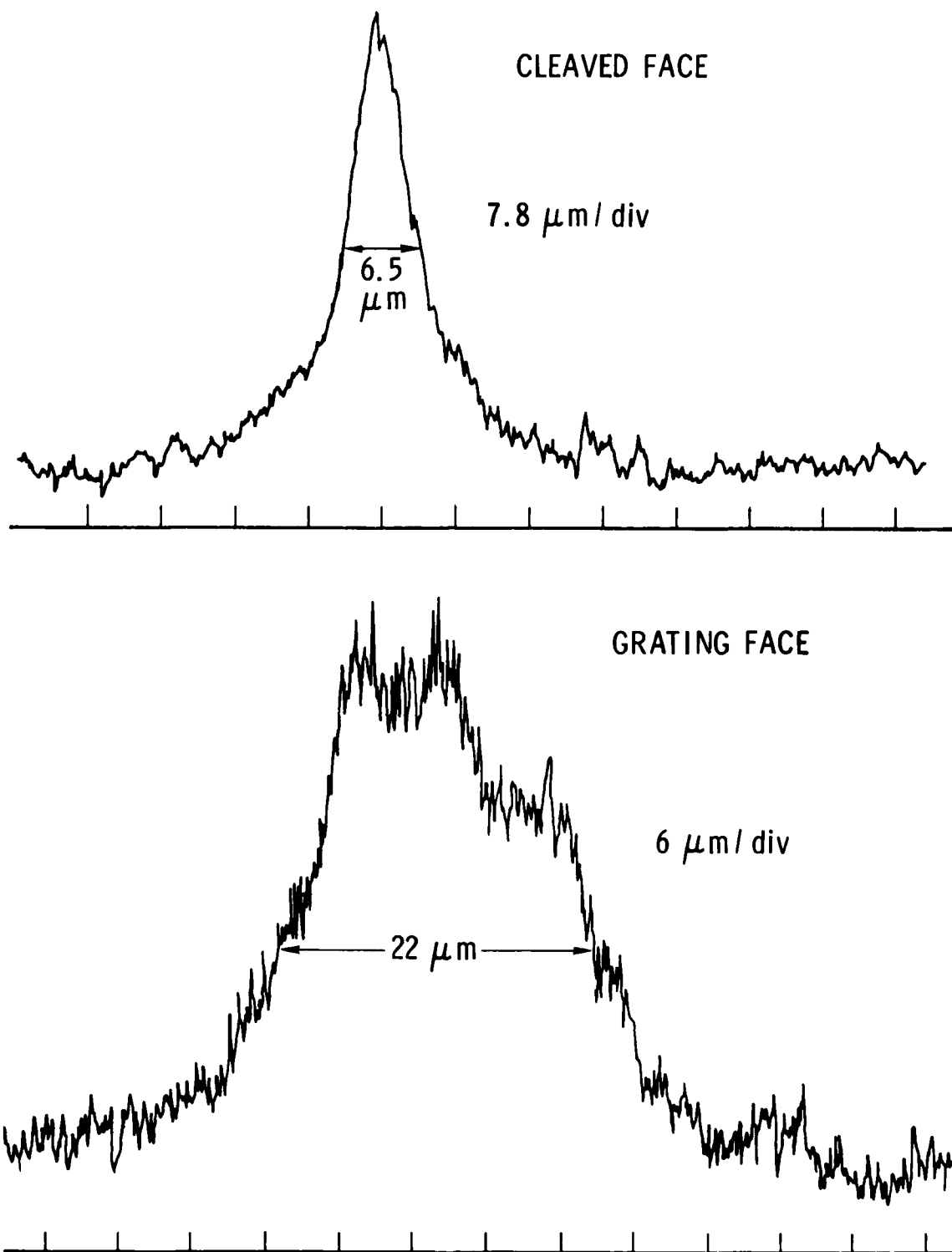


Figure 13 Diffraction-limited near-field patterns for the DBR laser output from diode g9 just above threshold.

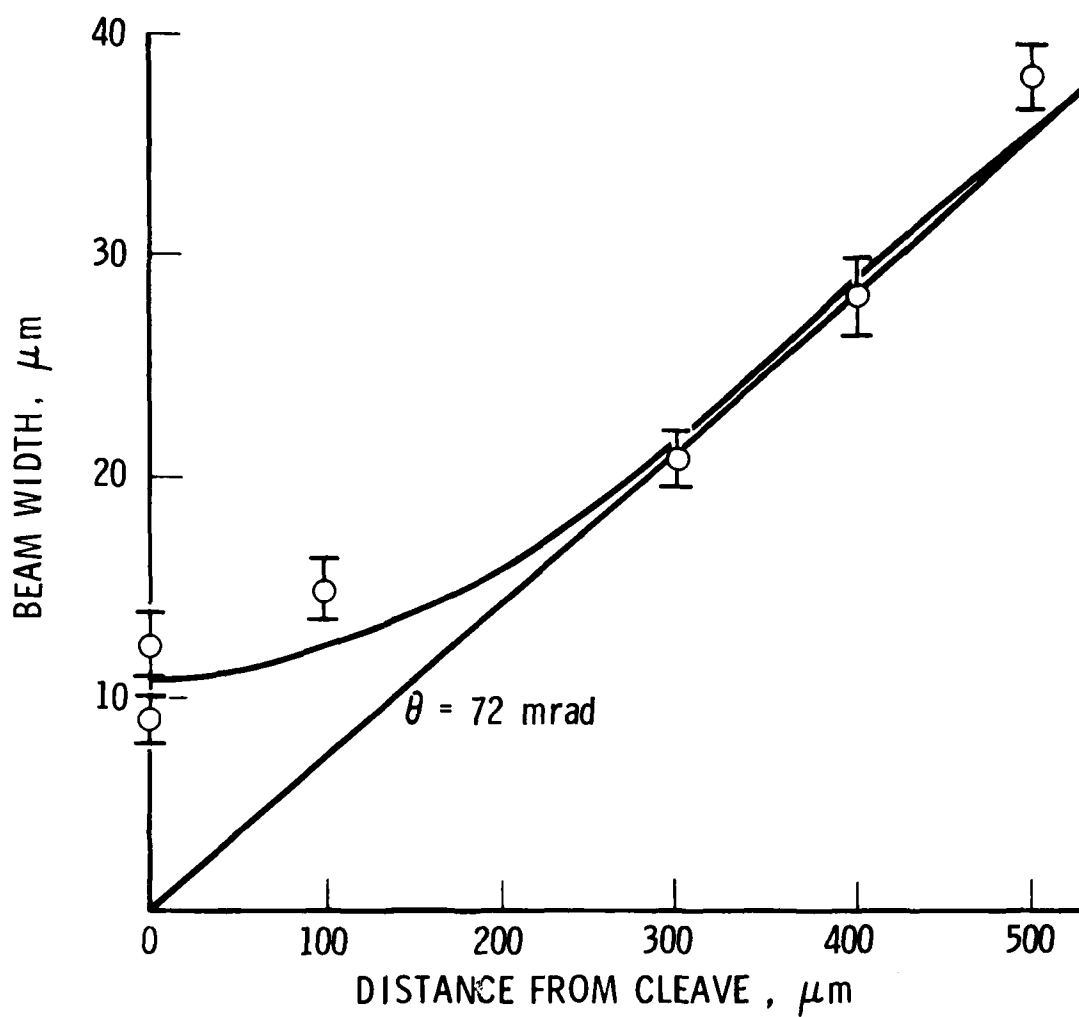


Figure 14 In-plane beam width as a function of distance from the exit face (as measured on a television monitor). Far field divergence angle is 72 m rad.

The laser output from the grating face was observed to have a near field profile which was a single filament $22\text{ }\mu\text{m}$ wide. This profile is the beam which has diffracted from the $5.4\text{ }\mu\text{m}$ filament in the laser region due to the use of a 1 mm long grating as shown in Fig. 15. If the filament is assumed to extend the length of the active region of the laser diode, and begins to expand when it enters the grating, then the diffraction should occur for a distance of 1 mm , at an angle given by the far field divergence angle divided by the index of refraction of the medium (0.02 rad). This divergence would cause the output of the grating to have a width of $20\text{ }\mu\text{m}$. This compares favorably with the measured filament width of $22\text{ }\mu\text{m}$.

For completeness, out-of-plane beam divergence was measured also. It was observed that the frequency corresponding to the higher order waveguide mode caused a double-humped far field pattern from the cleave. The divergence was greater than 0.48 rad and could not be measured since it was limited by the aperture of the lens which was used. The other frequency was a lowest order waveguide mode and had a beam divergence of 0.3 rad . This proves the assumption discussed earlier that the two frequencies are due to different modes occurring in the laser region.

Other diodes did not necessarily show in-plane diffraction limited behavior. The near field profiles of diode g5 are shown in Fig. 16. Although the apparent near field profile was $15\text{ }\mu\text{m}$ wide, the beam divergence was 0.16 rad , corresponding to a filament size of $2.4\text{ }\mu\text{m}$. In other words, the diode had a highly filamentary character which caused a great deal of beam divergence. This fact was made clear by looking at the profile out of the grating. The output had several filaments and an overall width of almost $100\text{ }\mu\text{m}$. Diodes such as this would not be very useful for signal processing applications because of large beam divergence.

The result of this study is the fact that although DBR lasers control the longitudinal modes, they do not improve the spatial modes or ensure diffraction limited operation. It is necessary to control the spatial modes in order to obtain diffraction limited guided beams which can be expanded and used for coupling to fiber optics and for signal processing. The spatial control must be obtained by the same techniques used in producing single mode Fabry-Perot lasers: narrow stripes, tapered junctions, and other modes control devices.

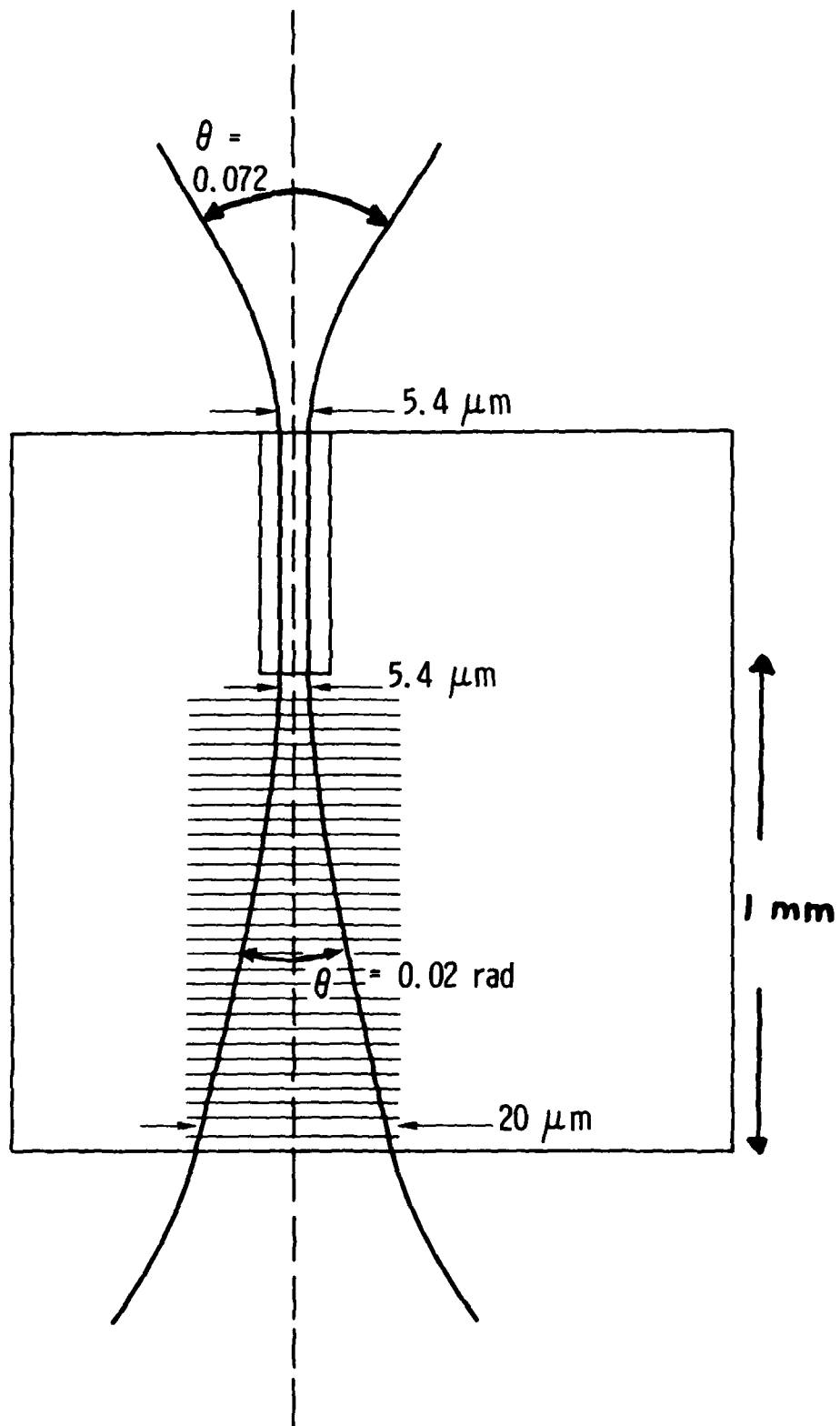


Figure 15 Diagram of top view of DBR laser, showing diffraction limited behavior of diode g9.

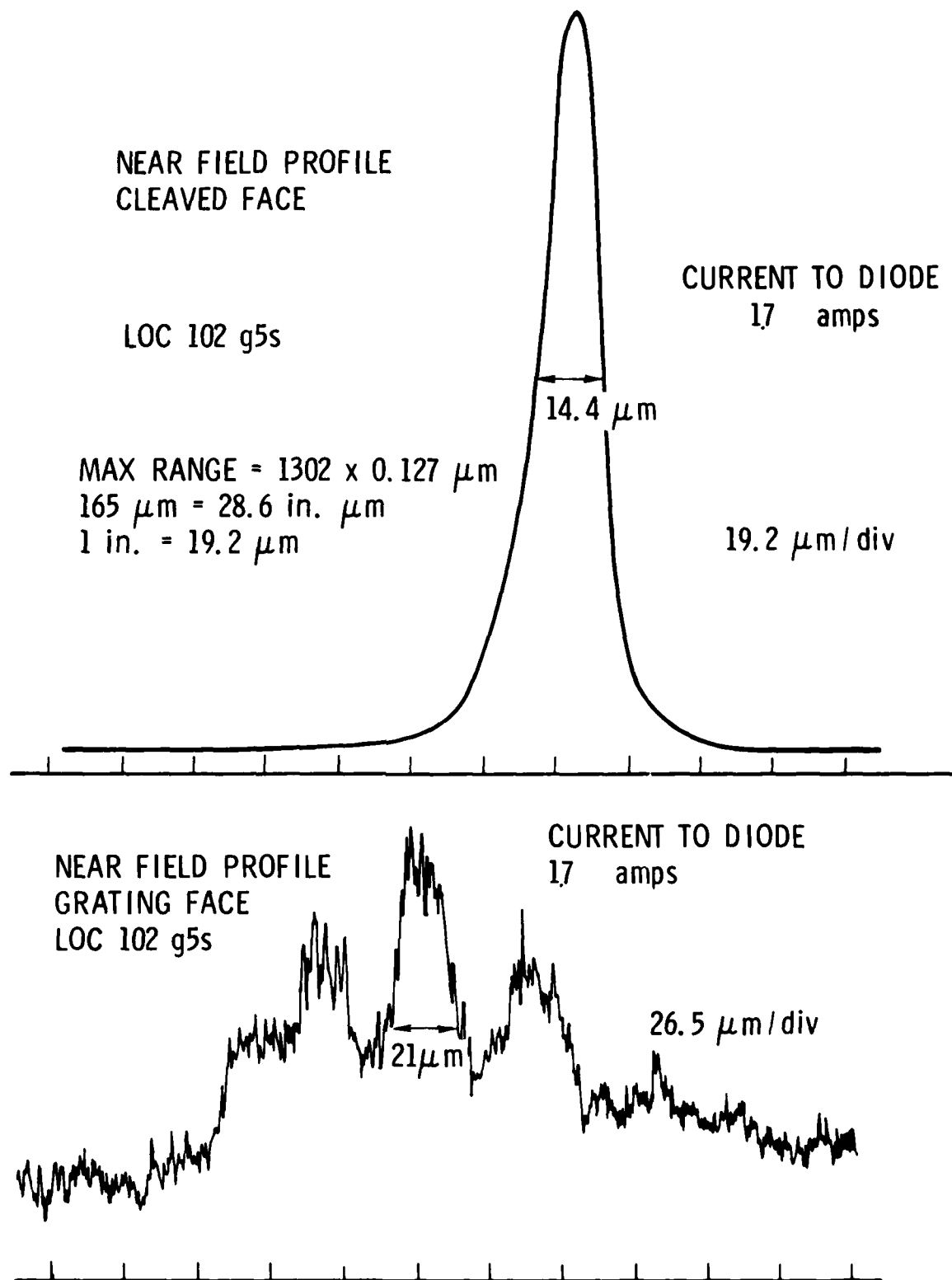


Figure 16 Near field profiles of diode g5, demonstrating non-diffraction-limited behavior, even right at threshold.

WAVEGUIDE BEAM EXPANSION

Beam expansion can be achieved by using a distributed Bragg deflector (DBD). This device consists of a corrugated waveguide, whose grating is slanted at an angle θ with respect to the incident beam. The geometry of the DBD is shown in Fig. 17. The incident beam enters from the left into a confined slab guide with a corrugated surface. Bragg reflection occurs from the grating, reflecting the beam at an angle equal to the incidence angle so that the total deflection angle $\theta_B = 2\theta$. However, the reflections from the corrugations add up coherently only if the Bragg condition is satisfied; that is,

$$\Lambda = \frac{\lambda_m}{2n \sin \theta}. \quad (8)$$

In addition to beam expansion, applications of the DBD include beam splitters (power division), deflectors (as, for example, to create ring geometries), polarizers and analyzers (with 90° deflection) and multiplexers/demultiplexers (with chirped gratings).

The theoretical analysis of the device has already been published.⁽²⁾ It was found that the incident light beam amplitude is reduced while travelling through the DBD region by an exponential factor with distance, $\exp(-\gamma z)$, due to deflection. The results of the calculation are:

$$\gamma_{TE} = \nu \cos^2 \theta_B \quad (9)$$

and

$$\gamma_{TM} = \nu \frac{2 n_2^2}{(n_2^2 - n_1^2)} \log \left(\frac{n_2}{n_1} \right) [\cos \theta_B - 1] - \cos^2 \theta_B, \quad (10)$$

where

$$\nu = w \frac{4\pi (n_2^2 - n_1^2) d^3}{3 (2\ell - 1) n_2 \lambda_o t_e^3} \quad (11)$$

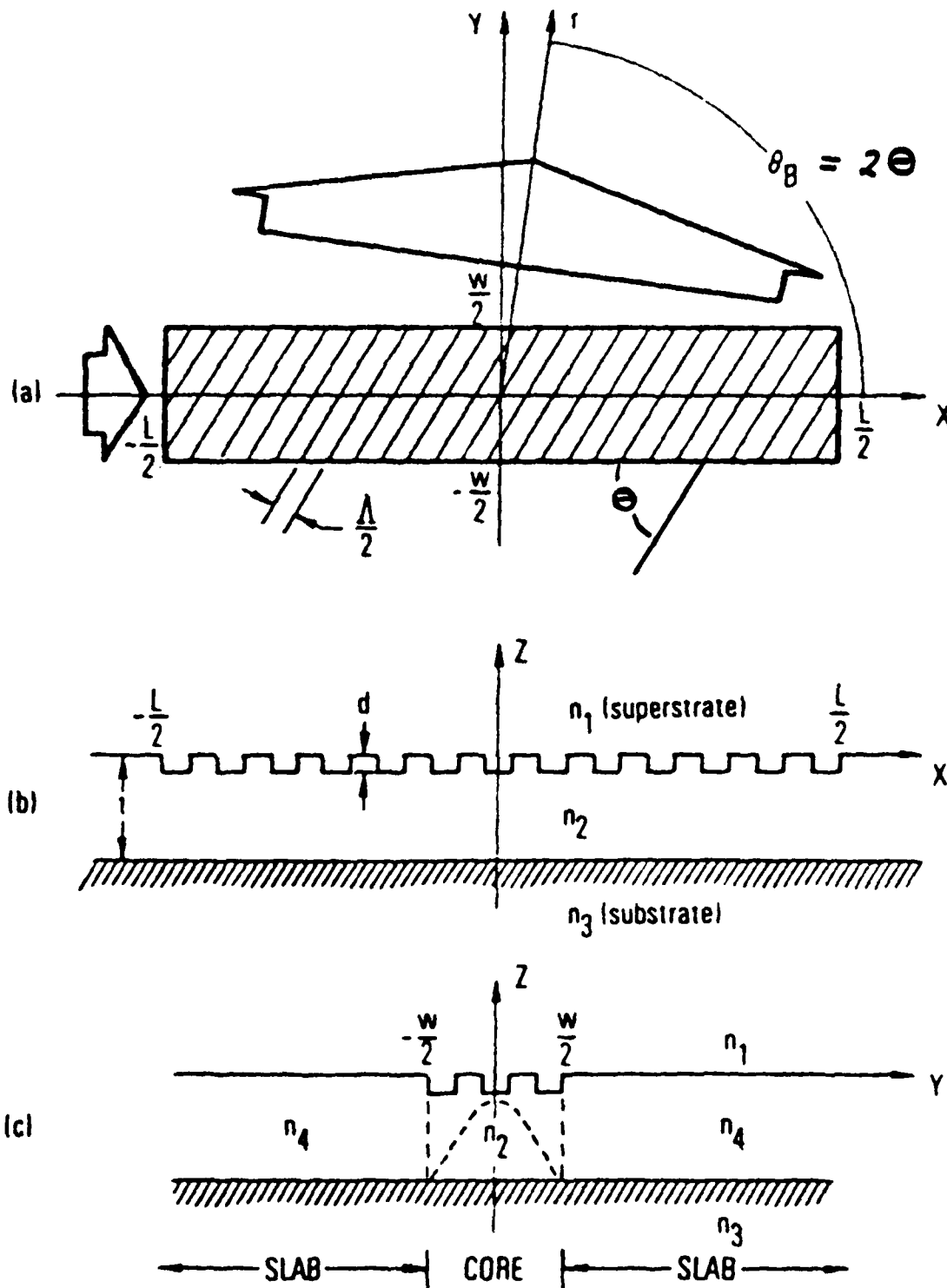


Figure 17 Distributed Bragg deflector: (a) top view; (b) side cross-sectional view; and (c) end cross-sectional view. Small and large (solid) arrows in (a) represent incident and deflected beams respectively. Dashed sinusoid in (c) represents equivalent core field distribution in the y direction.

The quantities are as defined in Fig. 17, with λ_0 the wavelength of incident light, ℓ the Bragg scattering order and t_e , the effective guide thickness. If the mode is near cutoff, $t_e = t + 1/\delta$, where δ is the exponential decay profile of the mode in the substrate.

Consider the deflection of a TM polarized beam at 90° , which is the configuration of greatest interest for beam expander applications:

$$\gamma_1 = \nu \frac{n_2^2}{n_2^2 - 1} \log n_2^2. \quad (12)$$

We have made use of the fact that $n_1 = \text{air} = 1$.

It is convenient to relate these results to those of retroreflection in a corrugated waveguide, given in Eq. 4. Plugging the expression for the coupling coefficient into the expression for ν , we write the DBD exponential coefficient as

$$\gamma_1 = \frac{4n_g^2 \log n_g^2}{\pi (n_g^2 - 1)} K_w^2. \quad (13)$$

Since the deflected beam has an amplitude which decreases with distance along the DBD according to an exponential with a coefficient γ , the intensity width of the expanded beam will be approximately $1/2\gamma$.

Defining the expansion factor as the width of the deflected beam divided by the incident beam width, we write the expansion factor as

$$\begin{aligned} F_1 &= \frac{1}{2\gamma_1 w} = 2 \frac{\pi (n_g^2 - 1)}{4n_g^2 \log n_g^2} \frac{L_g^2}{w} \\ &\equiv 2f^2 \left(\frac{L_g}{w} \right)^2 \end{aligned} \quad (14)$$

where we have defined the grating by its characteristic length, L_g

It can be seen that it is easy to obtain large expansion factors, since the characteristic length of gratings can be typically larger than w . Large expansion factors are of interest for the application described in Figure 2, the low beam divergence laser. Smaller expansion factors, however, are required for optical signal processing and fiber optics applications. In this

latter case, it is of interest to obtain expansion factors of roughly five, to expand the 20 μm emission from a GaAs stripe geometry laser to 100 μm beam, which could be used for signal processing or which could be used with an output grating coupler to make a beam which could be butt-coupled to multimode fibers, as shown in Figures 1 and 4. For the case of GaAs waveguides, $n_g = 3.6$, and $f = 0.56$. Thus expansion of a factor of 5 can be achieved if $L_g/w = 2.8$. For an incident beam of 20 μm , this requires $L_g = 56 \mu\text{m}$, or $K = .0089$. A grating with this coupling coefficient can be achieved if the waveguide is 1 μm thick and the tooth depth is 0.1 μm (Eq. 4).

Reflection with no expansion will occur when

$$w = \sqrt{2} \frac{\pi (n_g^2 - 1)}{4 n_g^2 \log n_g} L_g = \sqrt{2} f L_g. \quad (15)$$

For GaAs, $w = 0.79 L_g$ will ensure reflection with no expansion, at 90° deflection.

The research program was designed first to demonstrate beam expansion in high optical quality VPE GaAs waveguide material and then to apply the concept to LPE GaAs double heterostructures, so that the laser and beam expander could be combined into the same substrate.

Demonstration of beam expansion in VPE GaAs epilayers was successful. A perspective view of the Bragg-effect polarizer/analyzer which we fabricated is shown in Fig. 18. The asymmetric slab waveguide structure consisted of a 1 μm thick, n-type ($\sim 10^{16} \text{ cm}^{-3}$) GaAs layer epitaxially grown over a heavily doped n-type ($\sim 5 \times 10^{18} \text{ cm}^{-3}$) GaAs substrate; it supported only the lowest order one-dimensional, T.E. - and T.M. - polarized modes. Ninety degree Bragg scattering of the incident 1.15 μm radiation was accomplished via a second order periodic surface corrugation ($\Lambda = 0.478 \mu\text{m}$) which was ion milled into the waveguide surface and overcoated with a 0.1 μm thick layer of aluminum ($n_1^2 \approx -69$) in order to increase its deflection efficiency. As revealed by SEM examination of a cross section through the device, the corrugations bore a nearly triangular tooth profile. A photograph of a typical grating is shown in Fig. 19. The total corrugation length, L , and input beam width, w , were 3.2 mm and 50 μm , respectively.

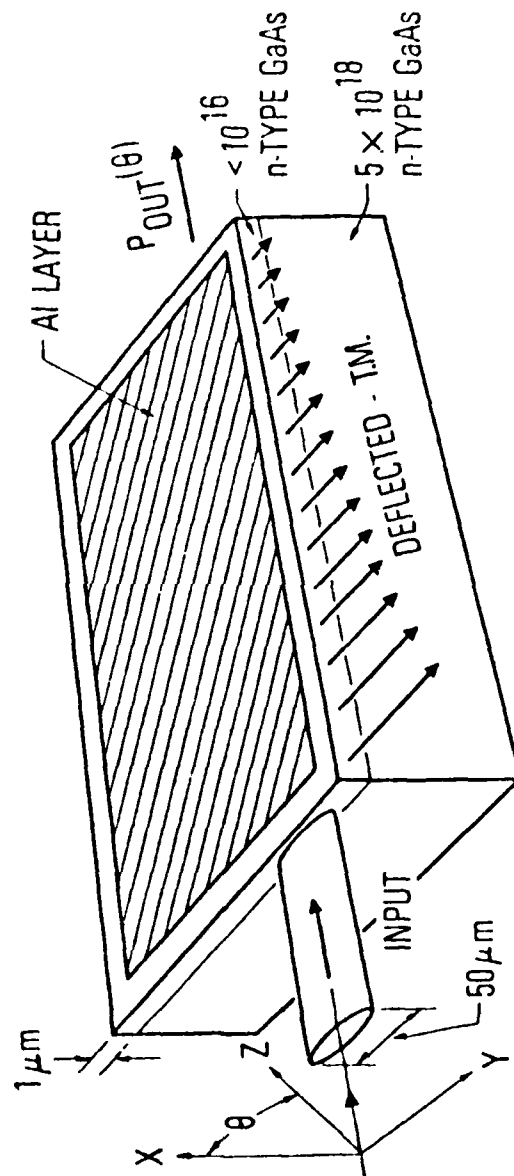


Figure 18 Perspective view of the Bragg-effect polarizer/analyzer which was tested. The electric field vector of the input beam is oriented at an angle θ to the waveguide surface normal.

Ion Milled Grating



0.5 μm PERIOD

Figure 19 Typical grating fabricated by ion milling through a photolithographically prepared photoresist mask

Figure 20 shows a semi-logarithmic plot of the near-field, deflected beam intensity profile of one of our 90° Bragg deflectors. The data shows that the deflected beam decreases a factor of 1/e in 1.3 mm length. With an input beam of 50 μm, this corresponds to an expansion factor of 38, much larger than required for fiber optics applications. From this data it can be inferred that the effective coupling length of the grating was $L_g = 385 \mu\text{m}$, with a coupling coefficient of $K = 0.0013$. This coupling is too weak for fiber optics applications. The reason for the weak effect is use of VPE GaAs. The index change due to the reduction of the number of free carriers in the epilayer is very small. As a result, the guided mode extends into the substrate and the effective guide width is larger than the 1 μm physical thickness of the epilayer. For the physical parameters used in the experiment, the effective guide thickness was several microns, causing the coupling coefficient to be small.

Because of the weakness of guiding in the VPE material, the effective waveguide thickness was large and the grating coupling coefficient was small. As a result, the expanded beam was too large to be useful for more than demonstration of the principles. However, it was demonstrated that even a grating with a low coupling coefficient can be used successfully as a polarizer-analyzer.⁽³⁾

Operation of the DBD as a polarizer/analyzer can be seen by observing that $\gamma_{TE} = 0$ for a deflection angle of 90°. Polarizer/analyzer performance parameters of interest include the extinction ratio, ρ , which we define as being equal to the ratio of T.M. - to T.E. -mode power deflected by the device, or

$$\rho = \frac{\gamma_{TM}}{\gamma_{TE}} \cdot \frac{\delta_{TE}}{\delta_{TM}} \cdot \frac{1 - \exp(-2 \delta_{TM} L)}{1 - \exp(-2 \delta_{TE} L)}, \quad (16)$$

and the T.M. deflection efficiency, η , which we define as being equal to the ratio of deflected to incident T.M. -mode power, or

$$\eta = \frac{\gamma_{TM}}{\delta_{TM}} [1 - \exp(-2 \delta_{TM} L)]. \quad (17)$$

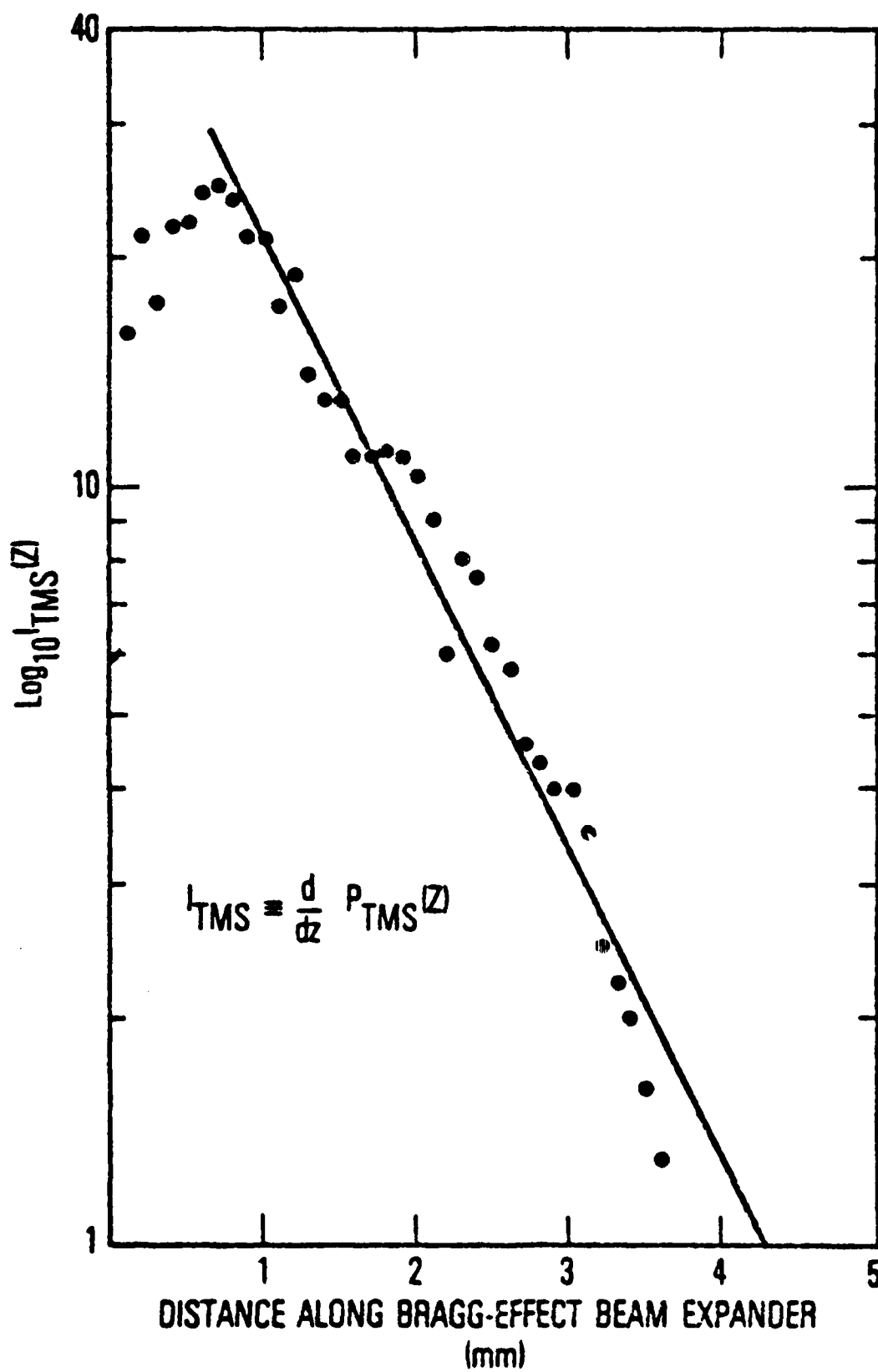


Figure 20 Semi-logarithmic plot of the near-field Bragg-scattered beam intensity profile of a 90° deflector.

In Eqs.(16) and (17), δ_{TE} and δ_{TM} are the total (including background) T.E. - and T.M. -mode attenuation coefficients, respectively, and L is the device length.

Experiments were performed on the polarization dependence of beam deflection using the VPE GaAs waveguide beam expander shown in Fig. 18. By measuring the near field intensity profile of the beam which was Bragg deflected by the polarizer/analyzer, δ_{TM} was determined to be 4.19 cm^{-1} . Knowledge of δ_{TM} together with measurements of the undeflected throughput power,

$$P_{out}(\theta) = P_{in} [\cos^2 \theta \exp(-2 \delta_{TM} L) + \sin^2 \theta \exp(-2 \delta_{TE} L)] \quad (18)$$

for $\theta = 0$ and $\pi/2$, were then used to yield $\delta_{TE} = 3.11 \text{ cm}^{-1}$, $\gamma_{TM} = 0.154 \text{ cm}^{-1}$, and $\eta = 0.034$. Finally, direct measurement yielded an extinction ratio of 343 from which it was inferred that $\delta_{TE} = 3.6 \times 10^{-4} \text{ cm}^{-1}$. Figure 21, which plots $P_{out}(\theta)$, $P_{TMS}(\theta)$ (the total T.M. power deflected), and the experimental data, summarizes the results.

The passive beam expander in VPE GaAs demonstrated that beam expansion was indeed possible using the Distributed Bragg Deflector. However, it was also demonstrated that the efficiency of deflection goes to zero for the TE mode at a deflection angle of 90° . This means that the 90° angle of deflection is not suitable for use in a monolithic circuit together with a DBR laser source. The DBR lasers we fabricated were found to operate with a TE polarization. This means that the angle of deflection must be some angle other than 90° . The most convenient angle of deflection is 45° .

Figure 22 shows a 45° DBD which was fabricated in VPE GaAs. The beam expansion is shown in the lower photograph, as a streak to the left of the beam. The difficulty in observing this device is the necessity of polishing the end face to obtain the output at 45° . The advantage is that the grating can be used in fundamental order. The deflection of the DBD in the VPE waveguide was very weak because the waveguide was so thick. Experiments on 45° deflection in thinner LPE GaAs waveguides await integration with DBR lasers.

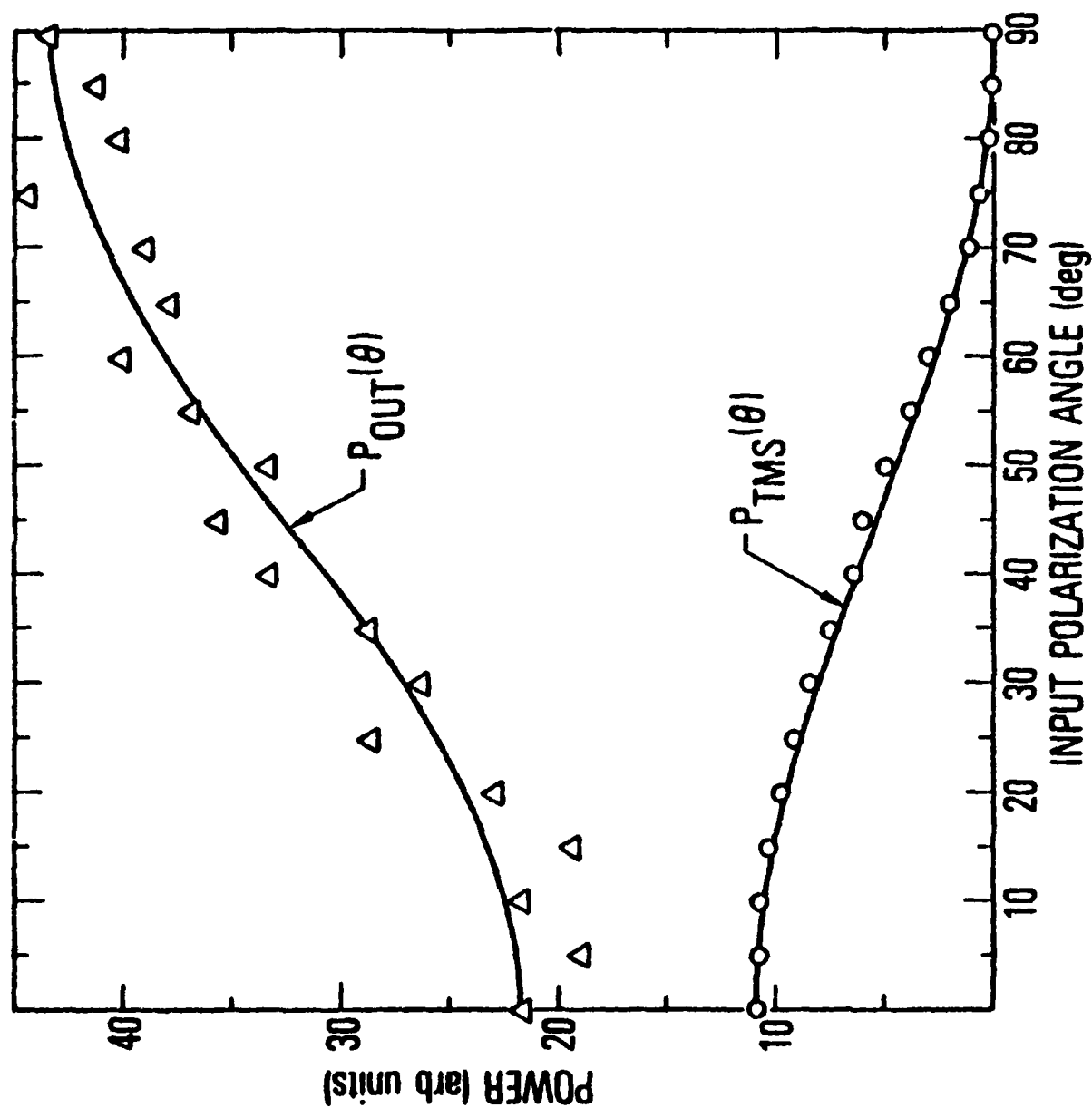


Figure 21 Plots of the throughput power, $P_{OUT}(\theta)$, and Bragg-scattered power, $P_{TMS}(\theta)$ as functions of the input beam polarization angle θ . Also shown are the experimental data (Δ and \circ).

45° Beam Expander

NEAR FIELD IMAGE
BEFORE AND AFTER ALIGNMENT

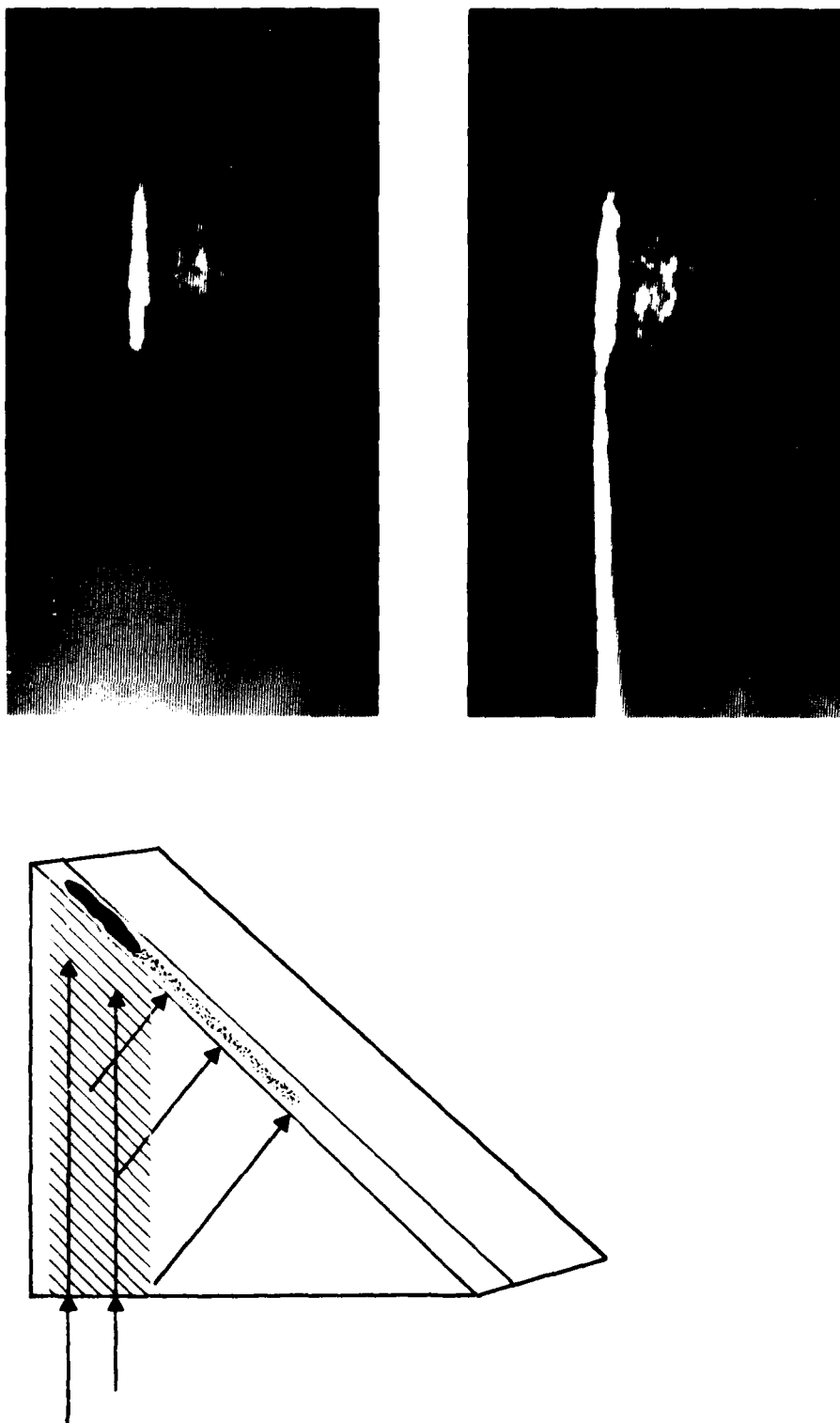


Figure 22 Geometry for 45° beam expander along with photographs of an IR television monitor of near field image of guided beam. The top photograph represents the unexpanded beam 50 μm wide before proper angular alignment. The bottom photograph demonstrates beam expansion with the streak to the left.

It is possible to use the results of the DBR lasers and the coupling coefficients of their gratings to predict the behavior for the 45° beam expander. The 45° beam expander used in conjunction with a GaAs DBR laser will be used with the grating in fundamental order and a spacing of 0.338 μm . To determine the expansion factor from the K value of the grating, we use Eq. (9) and obtain $\gamma_{\text{TE}} = (2K/\pi)^2 w \cos^2 \theta_B = w \cos^2 \theta_B / (\pi L_g)^2$. We wish to determine whether or not teeth of the shape used for the DBR laser can be satisfactory to produce beam expansion of the requisite factor of five. First we need to define an expansion factor, which includes the fact that the deflection is at an angle other than at 90°. The width of the expanded beam is $\sin \theta_B / (2 \gamma_{\text{TE}})$. This gives an expansion factor of

$$F_{\theta} = \frac{1}{2} \left(\frac{\pi L_g}{w} \right)^2 \frac{\sin \theta_B}{\cos^2 \theta_B}. \quad (19)$$

The expansion factor increases rapidly as $\theta \rightarrow 90^\circ$, but at this angle the TE reflectivity $\rightarrow 0$, so there is no inconsistency. When $\theta = 45^\circ$, the expansion factor will be

$$F_{45} = \left(\frac{\pi L_g}{w} \right)^2 / \sqrt{2}. \quad (20)$$

The DBR lasers we fabricated had an average $K = 0.0035$ and effective grating length $L_g = 140 \mu\text{m}$. From Eq. 4, it can be seen that the effective length of a grating used in first order differs from the effective length of a grating used in third order by a factor of 3. In first order these gratings would have $L_g = 47 \mu\text{m}$. From Eq. 20 it can be seen that for $w \sim 15 \mu\text{m}$, F_{45} is too large to produce a beam which will match into fibers. Appropriate beam expansion will require larger coupling coefficients K and smaller L_g . This requires developing heterostructure material with thinner waveguides, so that K may be made smaller. The DBR lasers we fabricated had waveguides of thickness $t = 1.6 \mu\text{m}$, while optimum structures would have waveguides of thickness $t = 0.6 \mu\text{m}$. Since $K \propto t^{-3}$, we can easily expect L_g to be more than eight times shorter. In first order $L_g \sim 6 \mu\text{m}$ is possible. Let us assume $w = 15 \mu\text{m}$ and we wish to expand into a $60 \mu\text{m}$ fiber. We are looking for $F_{45} = 4$. This will be possible with $L_g = 11 \mu\text{m}$, easily achievable.

Fabricating DBR lasers and 45° beam exapnders in material with waveguides $0.6\text{ }\mu\text{m}$ thick is the next step in the development of integrated optics lasers butt-coupled to fibers.

REFERENCES

1. "Laser Oscillation in Epitaxial GaAs Waveguides with Corrugation Feedback", M. Nakamura, H. W. Yen, A. Yariv, E. Garmire, S. Somekh, H. L. Gavin, Appl. Phys. Lett. 23 244 (1973).
2. "Distributed Bragg Deflector: A Multifunctional Integrated Optical Device", H. M. Stoll, Applied Optics 17, 2562 (1978).
3. "Bragg-effect Polarizer/Analyzers and Lens-less Waveguide Beam Expansion", H. M. Stoll, W. E. Soady, Proceedings of the Optical Society Topical Conference on Integrated Optics, January 1980.

LABORATORY OPERATIONS

The Laboratory Operations of The Aerospace Corporation is conducting experimental and theoretical investigations necessary for the evaluation and application of scientific advances to new military concepts and systems. Versatility and flexibility have been developed to a high degree by the laboratory personnel in dealing with the many problems encountered in the Nation's rapidly developing space systems. Expertise in the latest scientific developments is vital to the accomplishment of tasks related to these problems. The laboratories that contribute to this research are:

Aerophysics Laboratory: Aerodynamics; fluid dynamics; plasmadynamics; chemical kinetics; engineering mechanics; flight dynamics; heat transfer; high-power gas lasers, continuous and pulsed, IR, visible, UV; laser physics; laser resonator optics; laser effects and countermeasures.

Chemistry and Physics Laboratory: Atmospheric reactions and optical backgrounds; radiative transfer and atmospheric transmission; thermal and state-specific reaction rates in rocket plumes; chemical thermodynamics and propulsion chemistry; laser isotope separation; chemistry and physics of particles; space environmental and contamination effects on spacecraft materials; lubrication; surface chemistry of insulators and conductors; cathode materials; sensor materials and sensor optics; applied laser spectroscopy; atomic frequency standards; pollution and toxic materials monitoring.

Electronics Research Laboratory: Electromagnetic theory and propagation phenomena; microwave and semiconductor devices and integrated circuits; quantum electronics, lasers, and electro-optics; communication sciences, applied electronics, superconducting and electronic device physics; millimeter-wave and far-infrared technology.

Materials Sciences Laboratory: Development of new materials; composite materials; graphite and ceramics; polymeric materials; weapons effects and hardened materials; materials for electronic devices; dimensionally stable materials; chemical and structural analyses; stress corrosion; fatigue of metals.

Space Sciences Laboratory: Atmospheric and ionospheric physics, radiation from the atmosphere, density and composition of the atmosphere, aurorae and airglow; magnetospheric physics, cosmic rays, generation and propagation of plasma waves in the magnetosphere; solar physics, x-ray astronomy; the effects of nuclear explosions, magnetic storms, and solar activity on the earth's atmosphere, ionosphere, and magnetosphere; the effects of optical, electromagnetic, and particulate radiations in space on space systems.

DATE
FILMED
5-8